Systems/Circuits

Optogenetic Stimulation of the M2 Cortex Reverts Motor Dysfunction in a Mouse Model of Parkinson's Disease

Luiz Alexandre Viana Magno,[1] Helia Tenza-Ferrer,[1] Mélcar Collodetti,[1] Matheus Felipe Guimarães Aguiar,[1] Ana Paula Carneiro Rodrigues,[1] Rodrigo Souza da Silva,[1] Joice do Prado Silva,[1] Nycolle Ferreira Nicolau,[1] Daniela Valadão Freitas Rosa,[1] Alexander Birbrair,[4] Débora Marques Miranda,[1,3] and Marco Aurélio Romano-Silva[1,2]

[1]Centro de Tecnologia em Medicina Molecular, [2]Departamento de Saúde Mental, [3]Departamento de Pediatria, Faculdade de Medicina, Universidade Federal de Minas Gerais, Belo Horizonte, Brazil, and [4]Departamento de Patologia, Instituto de Ciências Biológicas, Universidade Federal de Minas Gerais, Belo Horizonte, Brazil 30130-100

Neuromodulation of deep brain structures (deep brain stimulation) is the current surgical procedure for treatment of Parkinson's disease (PD). Less studied is the stimulation of cortical motor areas to treat PD symptoms, although also known to alleviate motor disturbances in PD. We were able to show that optogenetic activation of secondary (M2) motor cortex improves motor functions in dopamine-depleted male mice. The stimulated M2 cortex harbors glutamatergic pyramidal neurons that project to subcortical structures, critically involved in motor control, and makes synaptic contacts with dopaminergic neurons. Strikingly, optogenetic activation of M2 neurons or axons into the dorsomedial striatum increases striatal levels of dopamine and evokes locomotor activity. We found that dopamine neurotransmission sensitizes the locomotor behavior elicited by activation of M2 neurons. Furthermore, combination of intranigral infusion of glutamatergic antagonists and circuit specific optogenetic stimulation revealed that behavioral response depended on the activity of M2 neurons projecting to SNc. Interestingly, repeated M2 stimulation combined with L-DOPA treatment produced an unanticipated improvement in working memory performance, which was absent in control mice under L-DOPA treatment only. Therefore, the M2-basal ganglia circuit is critical for the assembly of the motor and cognitive function, and this study demonstrates a therapeutic mechanism for cortical stimulation in PD that involves recruitment of long-range glutamatergic projection neurons.

Key words: **brain stimulation; cognition; movement; optogenetics; Parkinson's disorder; prefrontal cortex**

Significance Statement

Some patients with Parkinson's disease are offered treatment through surgery, which consists of delivering electrical current to regions deep within the brain. This study shows that stimulation of an area located on the brain surface, known as the secondary motor cortex, can also reverse movement disorders in mice. Authors have used a brain stimulation technique called optogenetics, which allowed targeting a specific type of surface neuron that communicates with the deep part of the brain involved in movement control. The study also shows that a combination of this stimulation with drug treatment might be useful to treat memory impairment, a kind of cognitive problem in Parkinson's disease.

Introduction

The activity balance of cortico-basal ganglia (CBG) connectivity is critical for motor functions and thus is closely involved in the movement disorder characteristic of Parkinson's disease (PD). A widely supported model suggests that loss of midbrain dopaminergic neurons in either PD patients or animal models triggers maladaptive changes in the CBG circuit organization, which modifies the excitatory input to basal ganglia and disrupt motor tone (Day et al., 2006; Pasquereau and Turner, 2011; Shepherd, 2013; Guo et al., 2015; de Hemptinne et al., 2015).

Whereas most PD therapeutic strategies target deep brain structures, including deep brain stimulation (DBS) and dopamine replacement therapy, there is increasing interest in cortical

Received Sept. 3, 2018; revised Feb. 1, 2019; accepted Feb. 4, 2019.

Author contributions: L.A.V.M., D.V.F.R., and M.A.R.-S. designed research; L.A.V.M., H.T.-F., M.C., M.F.G.A., A.P.C.R., R.S.d.S., J.d.P.S., N.F.N., D.V.F.R., D.M.M., and M.A.R.-S. performed research; L.A.V.M., D.V.F.R., A.B., and D.M.M. contributed unpublished reagents/analytic tools; L.A.V.M., H.T.-F., A.B., and M.A.R.-S. analyzed data; L.A.V.M. wrote the first draft of the paper; L.A.V.M., A.B., and M.A.R.-S. edited the paper; L.A.V.M. wrote the paper.

This work was supported by Fundação de Amparo à Pesquisa do Estado de Minas Gerais Grant FAPEMIG APQ 00476-14 and CNPq-Brazil to M.A.R.-S. L.A.V.M. was supported by a CAPES postdoctoral fellowship. We thank Prof. Karl Deisseroth and Dr. Maisie Lo for the optogenetic training at the Optogenetics Innovation Laboratory, Stanford University.

The authors declare no competing financial interests.

Correspondence should be addressed to Marco Aurélio Romano-Silva at romano-silva@ufmg.br.

https://doi.org/10.1523/JNEUROSCI.2277-18.2019

stimulation to alleviate PD symptoms (Beuter et al., 2014; Chou et al., 2015; Piano et al., 2018). For instance, electrophysiology and functional imaging studies suggest a cortical basis for the DBS efficacy through antidromic activation of pyramidal tract motor neurons (Li et al., 2012, 2014; de Hemptinne et al., 2015). DBS of subthalamic nucleus (STN) activates the motor cortex of PD patients (Weiss et al., 2015), and optogenetic stimulation of motorcortical M1 neuron terminals onto STN can relieve motor abnormalities in rodents (Gradinaru et al., 2009; Sanders and Jaeger, 2016). Moreover, cortical stimulation of PD patients has shown promising results (Drouot et al., 2004; Beuter et al., 2014; Chou et al., 2015; Udupa et al., 2016). Nevertheless, the mechanisms involved in cortical stimulation (including precise cortical subregions, subsets of neurons and downstream projection topography) remain unknown.

Cortical regions present a remarkable functional heterogeneity, containing distinct cell types and projection patterns (Harris and Shepherd, 2015; Gal et al., 2017). Specifically, the CBG network is spread, suggesting consideration of different sources of cortical synaptic inputs across this circuitry (Hintiryan et al., 2016). Likewise, this functional diversity implicates distinct behavioral outcomes derived from the CBG projection topography, which presumably can veil the most functionally relevant neurocircuit elements for therapeutic intervention. Surprisingly, no study to date has investigated a putative role for stimulation of glutamatergic neurons in the secondary (M2) cortex as a plausible target for PD therapy. This is particularly intriguing because M2 neurons monosynaptically innervate multiple basal ganglia structures, including striatum, STN, midbrain, and other brainstem areas, and receive reciprocal projections indirectly via large-scale loops (Watabe-Uchida et al., 2012; Gerfen et al., 2013; Hintiryan et al., 2016). Moreover, available evidence suggests that the altered prefrontal cortex in PD is characterized by atrophy (Zeighami et al., 2015) and abnormal connectivity (Borchert et al., 2016), which may be implicated in the slow acquisition of new motor skills observed in PD patients (Mentis et al., 2003; Wu and Hallett, 2005; Carbon et al., 2010).

Using an optogenetics approach, we identified a basal ganglia-projecting subpopulation of M2 glutamatergic neurons that were able to control motor behavior. This prompted us to investigate the therapeutic potential of this M2 circuitry in motor disturbances. Using a combined approach of anatomical tracing, optogenetic control, and behavioral recordings, we identified synaptic mechanisms that translate M2 stimulation into effective reversal of motor behavior dysfunction in the dopamine-depleted animal model of PD.

Materials and Methods

Animals

Male C57BL/6J mice were 6–7 weeks old at viral infusion. Animals were randomly allocated to the different experimental groups. All mice were housed in a temperature-controlled facility with a 12 h light/dark schedule and provided with food and water *ad libitum*. All animal protocols were performed following National Institutes of Health guidelines and approved by the Federal University of Minas Gerais (protocol 59/2014).

Surgical procedures

Mice were anesthetized with intraperitoneal injection of ketamine-xylazine (80 and 8 mg/kg, respectively) and placed into a stereotaxic frame (David Kopf Instruments). A mix of oxygen (1.0 L/min) and isoflurane at 1% was used to maintain a deep anesthetized state over the course of the surgery. Body temperature was controlled by a feedback heating pad throughout the procedure (David Kopf Instruments). The craniotomy was performed using a dental drill with a 0.75 mm burr. A pulled glass micropipette was used to inject (Nanoliter 2010, World Precision Instruments) the viruses into the M2 area: anteroposterior (AP), 2.5 mm from bregma; mediolateral (ML), ±1.0 mm; dorsoventral (DV), −1.5 and −1.0 mm. We injected a total of 1000 nl of viral suspension at an injection rate of 100 nl/min. These experiments were performed using AAV5/CaMKIIa-hChR2(H134R)-eYFP (ChR2-eYFP, titer 4×10^{12}) and AAV5/CaMKIIa-eYFP (eYFP, titer 4×10^{12}). For ChR2 expression in the population of M2 neurons that make synaptic contacts in the SNc (M2-SNc projection), mice were infected with adeno-associated viruses (AAVs) containing Cre-dependent ChR2-eYFP or eYFP (AAV/EF1a-DIO-hChR2(E123T/T159C)-EYFP, titer 4×10^{12} or AAV/EF1a-DIO-EYFP, titer 4×10^{12}) in M2 (AP: 2.5 mm; ML: ±1.0 mm; DV: −1.0 mm; injection volume 1000 nl), and WGA-Cre-mCherry (AAV/Ef1a-mCherry-IRES-WGA-Cre, titer 2×10^{12}) for retrograde expression of Cre recombinase in the SNc (AP: 3.0 mm; ML: ±1.5 mm; DV: −4.2 mm; injection volume 500 nl). All recombinant AAV vectors were packaged by Vector Core at the University of North Carolina. After injection, the micropipette was left in place for an additional 5 min and then slowly withdrawn. The skin was sealed with tissue adhesive (Vetbond, 3M), and ketoprofen (5 mg/kg) was injected subcutaneously once daily for 3 d. Mice were allowed to recover for 4 weeks after virus injection to allow axonal expression of opsin.

Chronic optical fiber implants were manufactured in ceramic LC ferrules sizing 200 μm of inner diameter and 230 μm of outer diameter (Plexon). The length of the fiber stubs was customized to be placed either above the layer 4/5 in the M2 (AP: 2.5 mm; ML: ±1.0 mm; DV: −1.0 mm) or above the M2 axons in the dorsomedial striatum (dmST; AP: 0.5 mm; ML: ±1.5 mm; DV: −3.2 mm). Fiber stubs were secured to the skull with Metabond (Parkell). Mice were allowed to recover for at least 1 week before habituation to the optogenetic devices. For experiments involving local drug infusion, a stainless-steel guide cannula (Plastics One) was implanted into the SNc (AP: 3.0 mm; ML: ±1.5 mm; DV: −3.2 mm), and a dummy cannula (Plastics One) was inserted to keep the fiber guide patent. This procedure was performed simultaneously with the fiber stub implant. Placements of the chronically implanted fiber and guide cannula were histologically verified for all experimental mice.

Drug treatments

For systemic treatment, haloperidol (D2-like receptor antagonist, 0.1 mg/kg) and SCH23390 (D1-like receptors antagonist, 0.05 mg/kg) were dissolved with 0.9% sterile NaCl immediately before use. Drugs were injected intraperitoneally at a volume of 10 ml/kg of body weight, 20 min before behavioral tests to cover the period of maximal drug (Kim et al., 2015). L-DOPA methyl ester (3.0 mg/kg) was administered intraperitoneally daily, starting 3 or 6 d previously to acute or chronic optogenetic sessions, respectively. An additional dose was injected 4 h before the photostimulation. For brain infusion experiments, mice were briefly head-restrained while a 33-gauge stainless-steel internal cannula (4.2 mm below pedestal, #C315IS-5/SPC, Plastics One) was inserted through the guide cannula previously implanted. The internal cannula was connected to a 1.0 μl Hamilton syringe fitted to a micropump via a polyethylene catheter. Awake mice received a 250 nl unilateral injection of 0.9% sterile saline or a solution containing NBQX (at 22.3 mM) and AP5 (at 38.04 mM) diluted in 0.9% sterile saline to antagonize AMPA and NMDA receptors, respectively. The pump flow was set at a constant rate of 100 nl/min. The internal cannula was removed 5 min after the termination of the injection. The dummy cannula was reinserted into the guide cannula, and mice were immediately placed in the open field apparatus. All drugs were purchased from Sigma-Aldrich.

Optogenetic manipulations

Illumination was powered by a blue LED light source (Plexon, 465 nm) mounted on a rotary joint placed in a fixed location above the behavior chamber. Lightweight optical patch cables (200 μm core and 230 μm cladding, Plexon) were used to connect the external portion of the fiber stubs to the light source. The light output was pulsed with a PlexBright 4-channel controller (Plexon). The light power output at the tip of the fiber stub (similar to the one implanted) was verified every day of the experiment using a powermeter (Thorlabs). Light intensity was calcu-

lated using the model based on direct measurements in mammalian brain tissue for predicting irradiance values developed by Deisseroth's laboratory (available at http://web.stanford.edu/group/dlab/cgi-bin/graph/chart.php). These calculations allowed us to adjust the light intensity to 71 mW/mm^2 for mice with fiber stubs into the dmST mice. For mice with the fiber stubs placed into M2 (M2 mice) or dmST mice treated with L-DOPA, we limited the estimated light intensity to 37.4 and 18.8 mW/mm^2, respectively, because greater intensities induced seizures. Light stimulation protocols were generated using the Radiant software (Plexon) with 10 ms pulse width at 20 Hz of light delivery. Optical stimulus in the bilateral experiment was adjusted to deliver the same amount of light to the two outputs.

Mice were first habituated to handling and patch cables in sessions that lasted 5 min, once per day for 2 d before experimentation began. Optogenetic sessions for experiments without drug treatment consisted of a 3 min acclimatization period followed by a 15 min period divided into five 3 min epochs, with the first (baseline locomotor activity), third and fifth epochs as light-OFF, and the second and fourth as the light-ON epochs (to record the effect of optogenetic modulation). Optogenetic sessions for experiments involving either drug treatments or unilateral dopamine depletion lasted 12 min (3 min for acclimatization following 3 min for each subsequent epoch: OFF, ON, OFF). Mice from bilateral dopamine depletion experiments were tested for 24 min (3 min for acclimatization, 9 min for the first light-OFF: prestimulation phase; 3 min for light-ON and another 9 min light-OFF epoch: poststimulation phase). During the light-ON epochs, mice received light stimulation for the entire period. At the end of the optogenetic session, mice were immediately detached from the light source and returned to their home cage. Groups were counterbalanced for order of light stimulation. One week later, the mice were tested again as described above under a lower light intensity protocol unless otherwise noted (see Results section).

Photostimulation for c-Fos induction and quantification of catecholamines were performed using a head-mounted wireless optogenetic device (HELIOS, Plexon) in each mouse inside its home cage (to minimize the unspecific neuronal activity due to exposition to the new context). Mice were first habituated to the test room and the wireless headstage over 3 d. On test days, mice were connected to the headstage and left undisturbed in the home cage. Three minutes later, the light was delivered wirelessly to the M2 for 1 min (465 nm, 37.4 mW/mm^2,10 ms square pulses at 20 Hz). We used the powermeter to adjust the LED power of the wireless device to deliver the same amount of light from the patch cables. We observed a similar light-evoked behavior response throughout these experiments compared with photostimulation using fiber optic cables. Mice were then killed either immediately for HPLC analyses or 90 min following the onset of photostimulation for c-Fos labeling.

Behavioral testing

Open field. Spontaneous rotational behavior, speed, mobile time, mobile episodes, and distance traveled in open field boxes (40 cm long, 40 cm wide, and 50 cm deep) was scored using an automated video-tracking software (ANYmaze, Stoelting). Rotational behavior (full 360° turns) was expressed as the percentage of ipsilateral (toward the side of the implant) or contralateral rotations relative to the total number of rotations over the period of testing. Mobile time and episodes were defined as periods (excluding rearing and sniffing) when the movement of the mouse center-point was >2.0 cm/s for at least 0.5 s (Kravitz et al., 2010; Parker et al., 2016). We found that all cases ($n = 7$) where the mice did not move after the light onset were due to misplacement of the fiber tip outside the M2-dmST projections and thus were excluded from analysis.

Cylinder test. The forelimb asymmetry was assessed in 10 min sessions. Mice were placed into a nonreflective glass cylinder (20 cm height, 9 cm diameter), and each time the rodent rose up and touched either paw (or both paws in simultaneous double contacts) to the wall of the cylinder was scored. The video recorded sessions were later scored manually using a slow-motion video player by an experimenter unaware of the treatment of the mouse. Data were expressed as a percentage of contralateral wall touches relative to the total number of ipsilateral and contralateral touches: (contralateral touches)/(ipsilateral touches + contralateral touches).

Y-maze. Spontaneous alternation performance was assessed based on the innate preference of animals to explore areas that have not been previously explored. This was measured by video monitoring the animal behavior during a single session in a Y-maze. The Y-maze apparatus consisted of three arms (30 cm long, 15 cm wide, and the walls were 30 cm high) made of wood covered with impermeable Formica. The patch cables were then connected to the animals yet inside their home cage, and 3 min later the mice were placed at the end of the start arm facing the wall. Mice were allowed to explore the three arms freely for 6 min. The session consisted of three 2 min epochs, with the first and, third epochs as the light-OFF epochs, and the second as the light-ON epoch. Entries into each arm, when all four paws were placed into the arm, were scored. Spontaneous alternation was defined as consecutive entries into each of the three arms without repetition. We defined the percentage of spontaneous alternation according to the following formula: percent alternation = [(number of alternations)/(total number of arm entries − 2)] × 100%.

Dopamine depletion and experimental design

Unilateral or bilateral depletion of dopamine was achieved through intracerebral injection of the neurotoxin 6-OHDA. To preserve noradrenergic neurons, desipramine-HCl (15 mg/kg, i.p., Sigma-Aldrich) was administered before surgery. Small aliquots of 6-OHDA-HBr (Sigma-Aldrich) were dissolved in ice-cold 0.02% ascorbic acid in sterile PBS (w/v) at a concentration of 3.2 μg/μl (free base). Solutions were freshly prepared for each injection. Each mouse received either unilateral or bilateral injections of 1.0 μl into the dmST (AP 0.5 mm, ML ±1.5 mm, DV −3.2 mm). We evaluated the dopamine-depleted mice through sessions distributed chronologically in the prelesion, postlesion, and photostimulation phases (described below).

Unilateral depleted mice. The prelesion phase consisted in collecting behavioral data on the seventh (D-7) and the third (D-3) days previous to the 6-OHDA and viral injections. All animals survived upon standard regimens of postoperative care. The postlesion phase began on the seventh postsurgical day (D+7) following 6-OHDA striatal infusion and lasted over a period of 4 weeks (until D+28). Open field tests were performed in weekly sessions while the cylinder tests were done only on D-3 (prelesion), D+28 (postlesion), and photostimulation phases (to prevent habituation to the apparatus). After behavior evaluation on D+28, fiber stubs were implanted (using the same coordinates of 6-OHDA infusion), and the mice were habituated to the patch cables through days 35–37. In these experiments, only mice showing at least 70% of spontaneous rotations in the ipsilateral direction were selected for the photostimulation phase (4 mice excluded). Photostimulation phase was performed on day 38 as previously described.

Bilateral depleted mice. The prelesion phase consisted of collecting behavioral data on the seventh (D-7) day previous to the striatal 6-OHDA infusions and the M2 viral injections. Exceptional postsurgical nursing was administered to these animals to ensure long-term recovery. During the first 10 postsurgical days, mice were allowed free access to sugared water (10 mM) and food pellets soaked in kitten milk replacement to stimulate appetite and gastrointestinal motility. During this period, we also administered daily 0.5 ml of lactated Ringer's solution (subcutaneously) to avoid dehydration (a common complication) and applied mucol gel to the penis to avoid prolapse. Bilateral lesions resulted in 16.6% mortality (4 of 24 injected mice). Behavioral evaluation of the postlesion phase was performed through open field tests on the 21st postsurgical day. The average speed of each mouse in the postlesion phase was normalized dividing them by the matched prelesion scores and only mice from the depleted group showing slower spontaneous movement (at least 30% decrease of average speed) were accepted for the photostimulation phase experiments (4 mice were excluded). Fiber stubs were implanted bilaterally into dmST, and the photostimulation phase was performed on day 30 as previously described.

Determination of dopamine and metabolites

Microdissected brain tissues were frozen on dry ice and stored at −80°C until analyzed. Dopamine (DA), 3,4-dihydroxyphenylacetic acid (DOPAC),

homovanillic acid (HVA), and norepinephrine (NE) content was measured from a single run by using ion-paired reversed-phase high performance liquid chromatography with electrochemical detection (HPLC-ECD) as described previously (Yang and Beal, 2011). Briefly, brains were homogenized in 0.1 M perchloric acid containing 50 ng/ml 2,3 dihydroxybenzylamine (DHBA). Samples were centrifuged at 18,000 × *g* for 15 min at 4°C, and supernatants were filtered through 0.22 μm PVDF membranes. We injected 40 μl of each sample into HPLC equipment (Shimadzu) equipped with a Discovery HS C18 column (150 mm × 4.6 mm, 3 μm; Sigma-Aldrich #569252-U) at a flow rate of 1 ml/min. Mobile phase consisted of 100 mM LiH_2PO_4, 1.5 mM 1-octanesulfonic acid, and 14% (v/v) HPLC grade methanol, and detection was performed using an L-ECD-6A detector (Shimadzu) at 800 mV. The chromatogram peak areas were calculated in the OpenChrome software, and quantification was performed by reference to a calibration of external standards. The results in ng/ml were normalized by concentration of total protein in mg/ml (BCA protein assay, Thermo Fisher Scientific). All chemical reagents were purchased from Sigma-Aldrich.

Histology

Mice were anesthetized with ketamine/xylazine (100 mg/kg per 10 mg/kg body weight) and transcardially perfused with ice-cold PBS, pH 7.4, followed by freshly prepared 4% PFA in PBS. Brains were postfixed for 12 h in 4% PFA at 4°C. Coronal or sagittal slices (50 μm thick) were prepared using a vibrating blade microtome (Leica Microsystems). The free-floating slices were washed with PBS and permeabilized with 0.1% Triton X-100 in PBS for 1 h, and then blocked with 2% BSA for 1 h and incubated overnight at 4°C in the same solution containing the following primary antibodies at the indicated dilutions: anti-NeuN (Millipore catalog #ABN91, RRID:AB_11205760, 1:2000), anti-tyrosine hydroxylase (Millipore catalog #AB152, RRID:AB_390204 or Abcam catalog #ab76442, RRID:AB_1524535, 1:1000), anti-c-Fos (Abcam catalog #ab208942, RRID:AB_2747772 or Santa Cruz Biotechnology catalog #sc-52, RRID:AB_2106783, 1:500), anti-VGluT2 (Millipore catalog #AB2251-I, RRID:AB_2665454, 1:1000), and anti-synaptophysin (Sigma-Aldrich catalog #S5768, RRID:AB_477523, 1:2000). After primary antibody incubation, slices were rinsed three times in PBS for 10 min each time and incubated for 2 h with the following AlexaFluor dye-conjugated secondary antibodies: AlexaFluor-488, -594, or -647 donkey anti-rabbit (1:3000), AlexaFluor-594 goat anti-chicken (1:3000), AlexaFluor-594 goat anti-guinea pig (1:3000), and AlexaFluor-594 goat anti-mouse (1:3000). Following incubation, the slices were washed three times with PBS and mounted in Prolong Gold medium (Thermo Fisher Scientific). Three-dimensional *z* stacks were acquired using a SP5 confocal microscope (Leica Microsystems). Acquisition settings were kept constant in each experiment for comparison between mice.

The axonal density was calculated according to previous studies (Oh et al., 2014; Lerner et al., 2015). Mice were injected unilaterally with AAV5/CaMKIIa-hChR2(H134R)-eYFP into the M2 (as described above). Six weeks later, slide-mounted coronal sections (50 μm thick) were obtained from perfused-fixed brains. We searched the eYFP projections in the full AP span of the brain, and confocal *z* stacks images covering a depth of 30 μm were acquired from each selected brain area. The selected brain areas for analysis included the major inputs located outside of the cortex and pons. The brain areas were selected as ROIs based on anatomical features in coacquired NeuN or NucRed Dead 647 images (Thermo Fisher Scientific). Confocal images were then background subtracted, converted to 8-bit, and then filtered with a Fiji threshold tool. The number of pixels was obtained from the Fiji-integrated density measurements. The projection percentage was calculated as ROI fluorescence divided by the total fluorescence into all regions (Oh et al., 2014). A mosaic of images was stitched together to represent the coronal views of the entire brain. Synaptic contacts of M2 axons were determined by the colocalization of punctuate eYFP-positive end terminals with the presynaptic protein synaptophysin. Colocalization experiments were performed in three confocal image stacks for each animal. Cells were manually counted using the Leica Application Suite Advanced Fluorescence software (LAS-AF, Leica Microsystems). To quantify levels of TH in the dmST, all images were captured under identical conditions and individual maximum *z*-projection images were stitched together to produce an entire region. Subdivision of the dorsal striatum into dorsomedial portion followed criteria from a previous study (Lerner et al., 2015). A mouse brain atlas (Franklin and Paxinos, 2008) was used to choose four representative coronal sections surrounding the 6-OHDA injection site of the striatum (AP 0.86, 0.5, 0.26, and 0.14 from bregma). Fluorescence of each image was measured as described above. The average number of TH-positive cells in the SNc was calculated in confocal *z* stack images acquired from two 50 μm coronal sections where the SNc was delineated from the VTA by localization of the medial lemniscus. These regional boundaries were defined *a priori*. Images were acquired over a strict depth of 30 μm for each slice, and TH-positive cells were manually counted using the LAS-AF software.

Experimental design and statistical analysis

For all datasets, normality was tested using the D'Agostino–Pearson omnibus test ($\alpha < 0.05$) and homogeneity of variance with Brown-Forsythe's test ($\alpha < 0.05$) to determine whether parametric or nonparametric analyses were required. For optogenetic sessions, all results were analyzed using two-way ANOVA with individual epochs as repeated measures and groups (experiment vs control) as independent variables. If a statistically significant effect was observed, *post hoc* testing with correction for multiple comparisons was performed using Sidak's multiple-comparisons test. One-way ANOVA followed by Bonferroni's multiple-comparisons tests was performed to compare three groups with a single variable. For two-sample comparisons of a single variable, we used the unpaired Student's *t* test. The experimenter was blinded to the experimental groups while running the statistical analysis. No statistical methods were used to predetermine sample sizes, but our sample sizes are similar to those reported in previous publications (Kravitz et al., 2010; Kim et al., 2017). For the exact number of animals used in each experiment and details of statistical analyses, see Results. All tests were two-tailed and had an α level of 0.05. All statistical analysis was performed using Prism version 6 (GraphPad Software).

Results

Neurocircuit organization of M2-projecting neurons

The M2 neurons are known to extend intertelencephalically providing bilateral inputs, or through the pyramidal tract by projecting axons ipsilaterally. To visualize the M2 neurons and their projection's density, the M2 cortex was infected with an AAV vector carrying the gene for the light-activated cation channel ChR2 driven by the calcium/calmodulin-dependent protein kinase II (CaMKII) promoter (AAV5/CaMKIIa-hChR2(H134R)-eYFP) (Fig. 1*a*,*b*).

It was observed that 75.15 ± 2.86% of the NeuN-positive cells within the injection site were transfected ($eYFP^+NeuN^+$ cells) (Fig. 1*c*, left); eYFP only: 0%; NeuN only: 24.85 ± 2.86%; $eYFP^+NeuN^+$ versus NeuN only mean difference (MD) = 50.31%, 95% CI 40.61–60.0 ($t_{(9)} = 15.22$, $p < 0.001$, $n = 4$, one-way ANOVA), and the vast majority of the ChR2-eYFP-positive cells overlapped with the glutamatergic presynaptic vesicle marker VGluT2 ($vGluT2^+eYFP^+$ cells) (Fig. 1*b*,*c*, right); eYFP only: 0.66 ± 0.10%; vGluT2 only: 3.62 ± 0.92%; $vGluT2^+eYFP^+$: 96.37 ± 0.92%; $vGluT2^+eYFP^+$ versus eYFP only MD = 95.71%, 95% CI 92.55–98.86 ($t_{(9)} = 89.01$, $p < 0.001$, $n = 4$, one-way ANOVA), indicating that most ChR2-positive neurons had an excitatory nature. The bodies of ChR2-eYFP-positive M2 neurons were distributed in all cortical layers except in layer I. ChR2-eYFP-positive cell bodies were mainly found in the M2 area, whereas a large number of labeled axons projected almost entirely ipsilaterally to subcortical structures (99.06% ipsilateral vs 0.94% contralateral; Fig. 1*d*–*g*). To identify the spatial patterns of the M2 projection, we examined the full AP span of the brain in coacquired nuclear- or synaptophysin-stained images. The projection fraction in brain areas where fluorescence

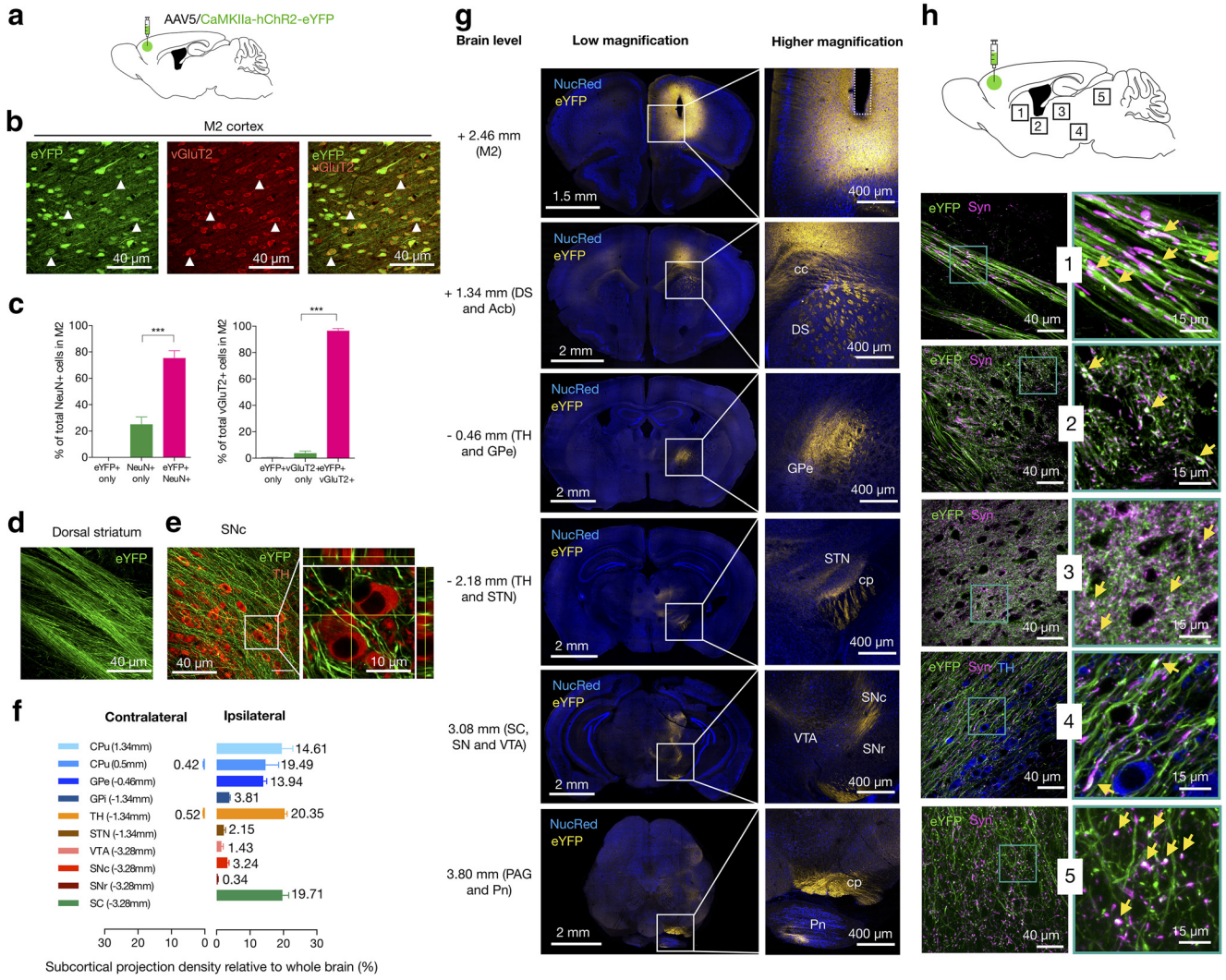

Figure 1. Neurocircuit organization of M2-projecting neurons. ***a***, Experimental scheme of the injection site in the M2 cortex and the virus used. Injections of AAVs expressing CaMKII-ChR2-eYPF were targeted unilaterally. Six weeks were allowed for AAVs to transduce and label cell bodies and projections. ***b***, In the M2 area, most eYFP-expressing neurons costained with the glutamatergic presynaptic vesicle marker VGluT2 at the injection site. Arrows indicate examples of eYFP $^{+}$vGluT2 $^{+}$ neurons. Green represents eYFP from AAV. Red represents vGluT2 from immunoreactivity. ***c***, Left, Percent of eYFP-positive of NeuN-identified cells within the injection site. Right, Percent of eYFP-positive of vGluT2-identified cells within the injection site. ***d***, ***e***, Representative sagittal planes showing M2 axons (eYFP in green) forming continuous bands through the dorsal striatum (on the left) to midbrain areas enriched in DA neurons (TH immunofluorescence in red, on the right). Inset, Representative maximum projection image with orthogonal views of eYFP-positive axons and TH immunofluorescence in the lateral part of the SNc. ***f***, Distribution of M2 projections in different subcortical areas. Bars represent the percentage of total projection volume (number of pixels per structure/total number of pixels per brain) in subcortical structures. Data were quantified in the 10 major brain subdivisions; fluorescence was detected in the injected (ipsilateral, on the right) and intact (contralateral, on the left) hemispheres (we excluded other cortical areas and pons from this measurement). Each bar represents the average projection signal from 4 mice at the indicated coronal levels. ***g***, M2 axons in the whole brain. Left column represents low-magnification sections displaying eYFP expression at different AP levels. Most of labeled M2 axons projected unilaterally to the dorsal striatum (DS), GPe, thalamus (TH), STN, SC, SN, VTA, and pontine nucleus (Pn). Right column: Insets, Axonal projection at higher magnification. Acb, Nucleus accumbens; cc, corpus callosum; cp, cerebral peduncle; PAG, periaqueductal gray. Yellow represents eYFP from AAV. Blue represents NucRed Dead labeling. ***h***, Merged low-magnification (left) and high-magnification (right, insets) representative sagittal images from dorsal striatum (1), GPe (2), thalamus (3), SNc (4), and SC (5) showing the colocalization of synaptophysin (Syn) immunoreactivity (magenta) in eYFP-positive (green) M2 axons. Yellow arrowheads indicate double-labeled presynaptic terminals (white). Summary data are indicated as mean ± SEM. ***$p < 0.001$.

was found was quantified in confocal *z* stack images as a proportion of the total eYFP fluorescence observed. M2 neurons innervated the dorsal part of the striatum (19.49 ± 2.29%), with a great projection fraction (34.1%) within the bounds of the dorsomedial subregion (more posterior). Major collaterals also projected into pallidum (GPe: 13.94 ± 0.60%; GPi: 3.81 ± 0.13), thalamus (TH: 20.35 ± 0.77%; STN: 2.15 ± 0.32), SNc (3.24 ± 0.29%), substantia nigra pars reticulata (SNr: 0.34 ± 0.08), superior colliculus (SC: 19.71 ± 1.10%), and pons (not included in the quantification analyses) (Fig. 1*f*). Notably, eYFP-labeled axons were absent in the ventral striatum, hippocampus, or hypothalamus. Overall, the regional axonal distribution of the M2 neurons was very similar across the animals. Interestingly, M2 anterograde projections formed continuous bands that extended through the dorsal striatum to midbrain areas enriched in DA neurons (Fig. 1*d*,*e*,*h*, sagittal planes). A few scattered axons were labeled in the VTA, whereas the areas of highest fluorescence located in the lateral part of the SNc where M2 axons also showed numerous spindle-like thickenings and terminal varicosities (Fig. 1*e*,*h*). We found that M2 neurons showed preferential contacts with aspiny dendrites of TH-positive neurons in the lateral SNc (Fig. 1*e*, inset). Terminal and *en passant* boutons M2 fibers colabeled with the presynaptic protein synaptophysin (Fig. 1*h*), which were densely present in the basal ganglia, thalamus, and SC, suggesting

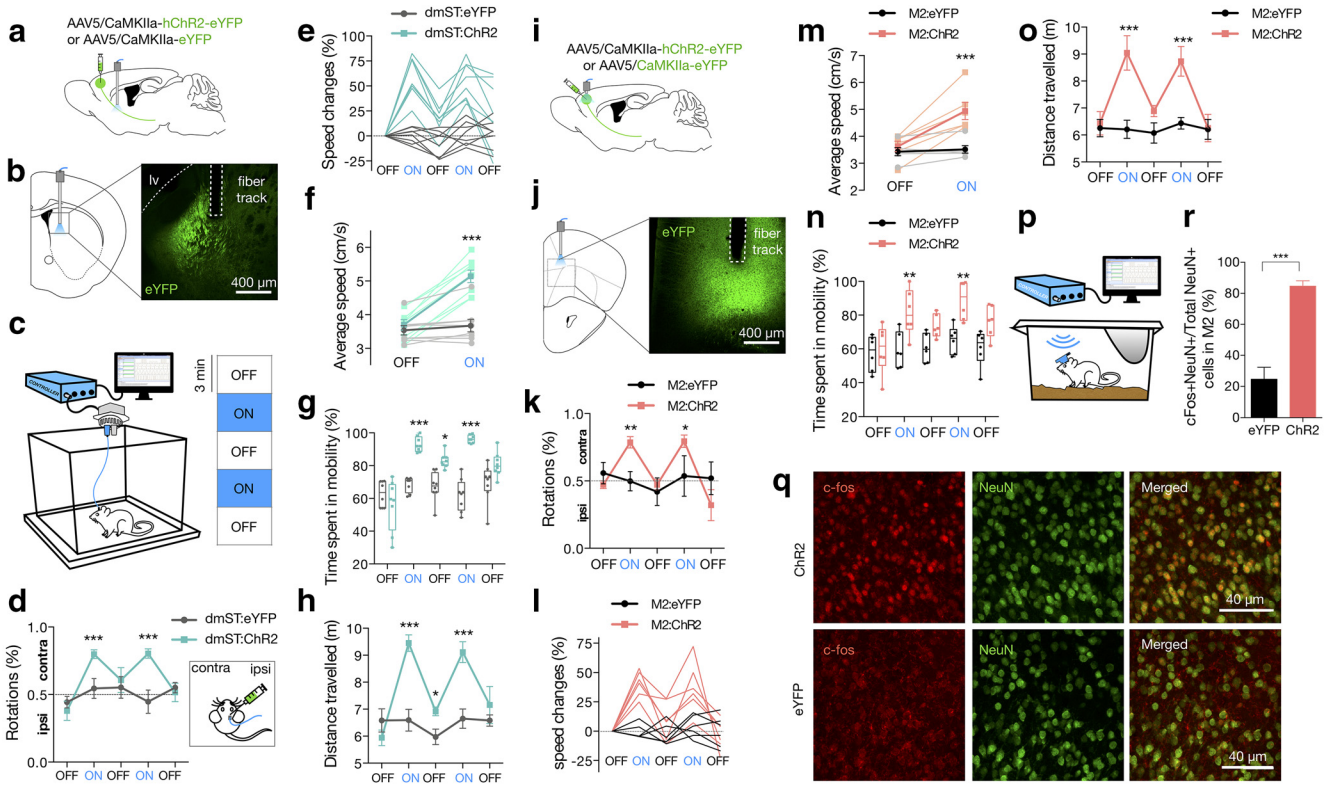

Figure 2. Optogenetic activation of M2 neurons induces locomotion. ***a***, Experimental scheme of the labeling approach to express either ChR2 (dmST:ChR2) or eYFP alone (dmST:eYFP) into the M2 area and to implant optical fiber over the dmST ($n = 8$/group). ***b***, Representative coronal image represents M2 axons and optical fiber placement (fiber track) in dmST. Green represents eYFP from AAV. lv, Lateral ventricle. ***c***, Illustration of the photostimulation setup used in the optogenetic sessions. Optogenetic testing consisted of five 3 min epochs with alternating light manipulation (OFF-ON-OFF-ON-OFF). ***d–h***, Photostimulation (465 nm, 71 mW/mm^2, 10 ms square pulses at 20 Hz) of dmST:ChR2 mice evoked transient increases in the (***d***) contralateral (contra) rotations (expressed as percentage of ipsilateral [ipsi] rotations relative to the total number of rotations), (***e***) changes of speed (relative to the first light-OFF epoch; lines indicate data for individual mice), (***f***) average speed (light colored lines represent data for individual mice, data from light-OFF epochs are pooled), (***g***) mobility time (as a percentage of the epoch duration), and (***h***) distance traveled during the light-ON periods, relative to the dmST:eYFP or the dmST:ChR2 group during the OFF epochs. ***i***, Experimental scheme of the labeling approach to express either ChR2 (M2:ChR2) or eYFP alone (M2:eYFP) and to implant optical fiber into the M2 area ($n = 6$/group). ***j***, Representative coronal image represents expression of ChR2-eYFP and optical fiber placement (fiber track) in M2. Green represents eYFP from AAV. ***k–o***, Photostimulation of M2:ChR2 (465 nm, 37.4 mW/mm^2,10 ms square pulses at 20 Hz) also increased (***k***) contralateral rotations, (***l***) changes in mean speed, (***m***) average speed, (***n***) mobility time, and (***o***) distance traveled during the light-ON periods, relative to the M2:eYFP and the M2:ChR2 group during the OFF epochs. ***p***, Illustration of the photostimulation setup using a head-mounted wireless optogenetic device inside the mice's home cage. ***q***, Representative images of M2 neurons expressing c-Fos after photostimulation in ChR2 (top) and eYFP (bottom) mice. Red represents c-Fos. Green represents eYFP (both from immunoreactivity). ***r***, Photostimulation increased the number of c-Fos-positive neurons within M2 in ChR2 animals compared with eYFP controls ($n = 6$/group). ***d***, ***e***, ***k***, ***l***, Dashed line indicates chance performance. Summary data are indicated as mean ± SEM. ***$p < 0.001$. **$p < 0.01$. *$p < 0.05$.

that these brain regions receive synaptic contacts from M2. According to our mapping, most of the M2 neurons were spatially organized as pyramidal tract neurons. Thus, the opsin-expressing M2 neurons project ipsilaterally to functionally connect the M2 cortex to brain areas critically involved in motor control.

Optogenetic activation of M2 neurons increases locomotion

To evaluate whether the M2 excitatory projections affect the locomotor behavior, mice received unilateral viral infusion with AAV5/CaMKII-ChR2-eYFP (ChR2) or AAV5/CaMKII-eYFP (eYFP, control); and 5 weeks later, an optical fiber was implanted above the M2 axons in the dmST (dmST:ChR2 or dmST:eYFP mice) (Fig. 2*a*,*b*).

One week after optical fiber implantation, the freely moving animals were monitored for changes in locomotor activity in response to the optogenetic excitation of M2 neurons. The optogenetic session consisted of a 3 min acclimatization period followed by a 15 min period divided into five 3 min epochs. The first (baseline locomotor activity), third and fifth epochs were the light-OFF, and the second and fourth were light-ON epochs (to record the effect of optogenetic modulation) (Fig. 2*c*). Compared with mice infected with control virus expressing eYFP only, photostimulation of dmST:ChR2 mice (465 nm, 71 mW/mm^2, 10 ms square pulses at 20 Hz) reliably evoked transient increases in the contralateral rotations during the light-ON periods (Fig. 2*d*; Movie 1; interaction effect$_{\text{light-epoch} \times \text{group}}$: $F_{(4,56)} = 3.78$, $p = 0.009$; main effect$_{\text{light-epoch}}$: $F_{(4,56)} = 4.44$, $p = 0.003$; main effect$_{\text{group}}$: $F_{(1,14)} = 9.17$, $p = 0.009$; $n = 8$/group, two-way repeated-measures ANOVA). This motor-evoked response was immediately after the light onset and was more evident in the first minute of stimulation. Photostimulation caused speed increments of 25% to 82.3% relative to the basal scores (Fig. 2*e*; interaction effect$_{\text{light-epoch} \times \text{group}}$: $F_{(4,56)} = 14.57$, $p < 0.001$; main effect$_{\text{light-epoch}}$: $F_{(4,56)} = 18.13$, $p < 0.001$; main effect$_{\text{group}}$: $F_{(1,14)} = 29.33$, $p < 0.001$; $n = 8$/group, two-way repeated-measures ANOVA). On average, we found that speed during the light-ON periods was significantly greater than in light-OFF epochs (Fig. 2*f*; interaction effect$_{\text{light-epoch} \times \text{group}}$: $F_{(1,14)} = 100.5$, $p < 0.001$; main effect$_{\text{light-epoch}}$: $F_{(1,14)} = 147.0$, $p < 0.001$; main effect$_{\text{group}}$: $F_{(1,14)} = 12.71$, $p = 0.003$; $n = 8$/group, two-way repeated-measures ANOVA). The dmST:ChR2 mice also spent more time in mobility (Fig. 2*g*; interaction effect$_{\text{light-epoch} \times \text{group}}$: $F_{(4,56)} = 16.08$, $p < 0.001$; main effect$_{\text{light-epoch}}$: $F_{(4,56)} = 20.01$, $p < 0.001$; main effect$_{\text{group}}$: $F_{(1,14)} = 36.67$, $p < 0.001$; $n = 8$/group, two-way repeated-measures ANOVA), and exhibited an increase in

Movie 1. Photostimulation of dmST-ChR2 mouse, related to Figure 2*a–h*.

total distance traveled during the light-ON epochs (Fig. 2*h*; interaction effect$_{\text{light-epoch} \times \text{group}}$: $F_{(4,56)} = 13.50$, $p < 0.001$; main effect$_{\text{light-epoch}}$: $F_{(4,56)} = 17.44$, $p < 0.001$; main effect$_{\text{group}}$: $F_{(1,14)} = 9.39$, $p = 0.008$; $n = 8$/group, two-way repeated-measures ANOVA).

In a separate group of animals, we also investigated the effect of photostimulation in mice implanted with fiber stubs in the core area of the injection site (M2:ChR2 or M2:eYFP mice) (Fig. 2*i*,*j*). These animals presented relatively similar behavior patterns in response to the optogenetic stimulation (465 nm, 37.4 mW/mm^2, 10 ms square pulses at 20 Hz). In contrast, we found less pronounced light-evoked effects on average speed, and distance traveled compared with dmST-ChR2 mice (Fig. 2*k–o*; % of rotations: interaction effect$_{\text{light-epoch} \times \text{group}}$: $F_{(4,40)} = 3.45$, $p = 0.016$; main effect$_{\text{light-epoch}}$: $F_{(4,40)} = 3.84$, $p = 0.001$; main effect$_{\text{group}}$: $F_{(1,10)} = 0.74$, $p = 0.408$; changes in mean speed: interaction effect$_{\text{light-epoch} \times \text{group}}$: $F_{(4,40)} = 9.12$, $p < 0.001$; main effect$_{\text{light-epoch}}$: $F_{(4,40)} = 11.14$, $p < 0.001$; main effect$_{\text{group}}$: $F_{(1,10)} = 22.15$, $p < 0.001$; average speed: interaction effect$_{\text{light-epoch} \times \text{group}}$: $F_{(1,10)} = 22.64$, $p < 0.001$; main effect$_{\text{light-epoch}}$: $F_{(1,10)} = 29.03$, $p < 0.001$; main effect$_{\text{group}}$: $F_{(1,10)} = 8.98$, $p = 0.013$; mobility time: interaction effect$_{\text{light-epoch} \times \text{group}}$: $F_{(4,40)} = 4.39$, $p = 0.005$; main effect$_{\text{light-epoch}}$: $F_{(4,40)} = 10.88$, $p < 0.001$; main effect$_{\text{group}}$: $F_{(1,10)} = 9.66$, $p = 0.01$; and distance traveled: interaction effect$_{\text{light-epoch} \times \text{group}}$: $F_{(4,40)} = 9.93$, $p < 0.001$; main effect$_{\text{light-epoch}}$: $F_{(4,40)} = 11.89$, $p < 0.001$; main effect$_{\text{group}}$: $F_{(1,10)} = 6.95$, $p = 0.025$; $n = 8$/group, two-way repeated-measures ANOVA).

We measured the expression of the activity-dependent immediate early gene c-Fos to track the activation of M2 neurons in response to light. To minimize the unspecific neuronal activity due to exposition to the open field, photostimulation for c-Fos induction was performed using a head-mounted wireless optogenetic device in each mouse inside its home cage 1 week following the first trial (Fig. 2*p*). Light was wirelessly triggered and delivered to the M2 for 1 min (465 nm, 37.4 mW/mm^2, 10 ms square pulses at 20 Hz). We found that this manipulation also produced a similar light-evoked behavior response compared with the wired setup. Mice were then killed 90 min following the onset of photostimulation for c-Fos labeling. Compared with the eYFP group, we found a significantly higher proportion of neurons double-immunolabeled for c-Fos and NeuN just below the placement of the optical fiber in ChR2 mice (Fig. 2*q*,*r*; eYFP: 24.62 ± 3.14%; ChR2: 84.67 ± 1.39%; MD = 60.05, 95% CI 52.40–67.71, $t_{(10)} = 17.48$, $p < 0.001$, $n = 6$/group, Student's *t* test). Together, these data indicate that optogenetic activation of either M2 neuronal bodies or their axons into the dmST evoke locomotor activity.

M2-dmST projection relies on basal ganglia neurotransmission to promote locomotion

As M2 neurons project to the basal ganglia structures, including areas enriched in dopaminergic (DA) neurons in the SNc (Fig. 1*e–h*), we next investigated the role of DA neurotransmission on the light-elicited locomotor behavior. We first photostimulated an independent group of dmST:ChR2 mice with light pulse trains over 1 min, and the catecholamine content was determined in the M2, dorsal striatum, and midbrain immediately after wirelessly brain illumination. Tissue levels of DA and its metabolites DOPAC and HVA were increased in stimulated striatum or midbrain, relative to the sham stimulated hemispheres (Fig. 3*a–c*; stimulation vs sham in ng/mg of protein, dorsal striatum: DA: 1.254 ± 0.09 vs 1.735 ± 0.10, $t_{(6)} = 3.516$, $p = 0.013$; DOPAC: 1.191 ± 0.09 vs 1.678 ± 0.11, $t_{(6)} = 3.327$, $p = 0.016$; HVA: 0.818 ± 0.26 vs 1.390 ± 0.12, $t_{(6)} = 1.995$, $p = 0.093$; midbrain: DA: 0.8125 ± 0.07 vs 1.228 ± 0.10, $t_{(6)} = 3.43$, $p = 0.014$; DOPAC: 0.5605 ± 0.03 vs 0.8766 ± 0.04, $t_{(6)} = 5.71$, $p = 0.001$; HVA: 0.4995 ± 0.20 vs 0.9665 ± 0.15, $t_{(6)} = 1.842$, $p = 0.115$; $n = 4$/group, Student's *t* test). No significant change in the M2 or for norepinephrine levels overall was observed (Fig. 3*a–c*). Although we did not provide a direct assessment of extracellular monoamine release *in vivo*, increased DA and its metabolites in the basal ganglia support the notion that the DA neurotransmission might influence the behavioral consequences of the optogenetic stimulation.

We next examined whether selective inhibition of DA receptors could prevent the light-induced locomotor behavior. Three different groups of dmST:ChR2 mice were treated with either vehicle or the D2R and D1R dopamine receptors antagonists haloperidol (0.1 mg/kg, i.p.) and SCH23390 (0.05 mg/kg, i.p.), respectively, 20 min before the brain illumination. Although the drugs only attenuated the light-induced rotational asymmetry (Fig. 3*d*; contralateral rotations interaction effect$_{\text{light-epoch} \times \text{group}}$: $F_{(4,24)} = 1.254$, $p = 0.3153$; % of contralateral rotations MD, light-ON vs light OFF: ChR2-Sal: 32.0, $p = 0.001$; ChR2-HAL: 19.20, $p = 0.049$; ChR2-SCH23390: 16.80, $p = 0.042$; $n = 5$/group, two-way repeated-measures ANOVA), both haloperidol and SCH23390 abolished the increases of speed in response to light stimuli (Fig. 3*e*; average speed interaction effect$_{\text{light-epoch} \times \text{group}}$: $F_{(2,12)} = 12.46$, $p = 0.0012$; average speed [cm/s] MD, light-ON vs light OFF: ChR2-Sal: 1.36, $p < 0.001$; ChR2-HAL: −0.038, $p > 0.99$; ChR2-SCH23390: 0.092, $p > 0.99$; $n = 5$/group, two-way repeated-measures ANOVA).

We then performed a chronic L-DOPA treatment (4 d of daily injection of 3 mg/kg, i.p.) to increase the striatal content of DA. Mice injected with L-DOPA displayed a 68% increase in the DA

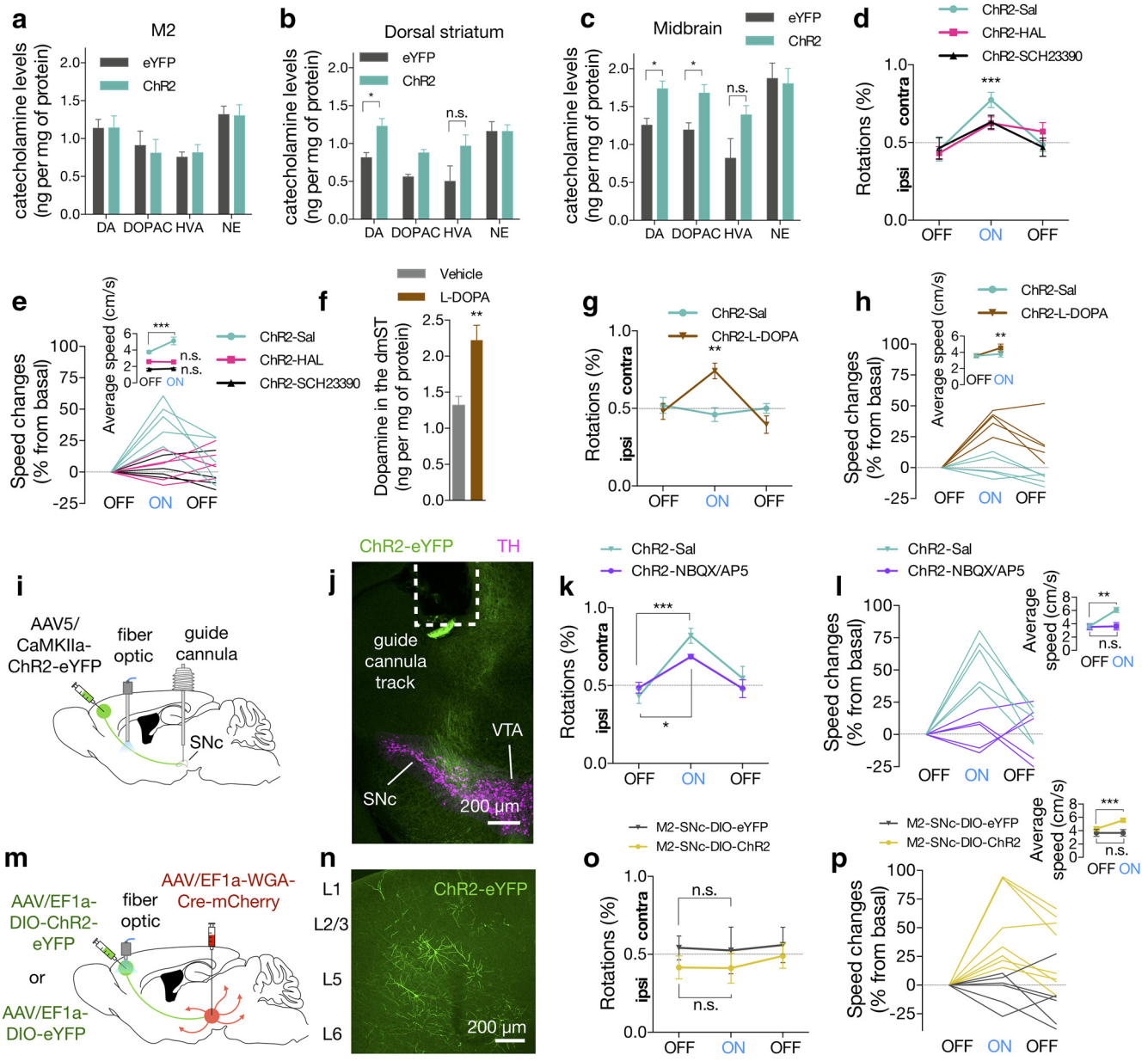

Figure 3. M2-dmST projection relies on basal ganglia neurotransmission to promote locomotion. ***a–c***, Optogenetic stimulation of dmST:ChR2 mice ($n = 4$) increased tissue concentrations of DA and DOPAC, relative to the eYFP group ($n = 4$). The changes were observed in the dorsal striatum and midbrain measured immediately after photostimulation session. ***d***, ***e***, Pretreatment with the D2R antagonist haloperidol (ChR2-HAL, $n = 5$) and D1R antagonist SCH23390 (ChR2-SCH23390, $n = 5$) equally attenuated the light-evoked increases in the contralateral (contra) rotations compared with saline-treated animal (ChR2-Sal, $n = 5$) (top, expressed as percentage of ipsilateral [ipsi] rotations relative to the total number of rotations) and blocked the changes of speed (bottom, relative to the first light-OFF epoch; lines indicate data for individual mice) and average speed (inset). ***f***, Mice injected with L-DOPA ($n = 4$) displayed a 68% increase in the DA levels, relative to vehicle-treated animals ($n = 4$). ***g***, ***h***, Treatment with L-DOPA potentiated the locomotor behavior as it decreased the minimum light power intensity (18.8 mW/mm^2 vs 71 mW/mm^2 in Fig. 2*d–h*) necessary to elicit the contralateral rotations, changes of speed, and average speed ($n = 5$/group). ***i***, A schematic diagram of the experimental approach to deliver ChR2 in the M2, place optical fiber in the dmST and inject glutamate antagonists into SNc. ***j***, Representative coronal image represents M2 axons in the midbrain and guide cannula placement ~1.0 mm above SNc. Green represents eYFP from AAV. Magenta represents TH immunoreactivity. ***k***, ***l***, Infusion of NBQX/AP5 (AMPA/NMDA receptor antagonists, respectively) into the SNc attenuated contralateral rotations and ablated changes of speed and average speed (inset) elicited by photostimulation ($n = 5$/group). ***m***, Schematic diagram of the experimental approach to deliver Cre-dependent ChR2 or EYFP in the M2, and WGA-Cre in the SNc. Optical fiber was placed in M2. ***n***, Representative sagittal image represents a subset of M2 neurons (green) in the cortical layer 5 (L5) that makes synaptic contact within SNc (M2-SNc circuit). ***o***, ***p***, Stimulation of M2-SNc neurons expressing ChR2 did not evoke rotational behavior but induced speed increments ($n = 6–8$/group). In all figures, summary data are indicated as mean ± SEM. ***d***, ***e***, ***g***, ***h***, ***k***, ***l***, ***o***, ***p***, Dashed line indicates chance performance. ***$p < 0.001$. **$p < 0.01$. *$p < 0.05$.

concentration, relative to vehicle-treated animals (Fig. 3*f*); DA in ng/mg of protein: 1.32 ± 0.12 in Sal vs 2.22 ± 0.20 in L-DOPA, $t_{(6)} = 3.727$, $p = 0.001$, $n = 4$/group, Student's t test). Remarkably, we noticed that the minimum light power intensity necessary to elicit the contraversive movement and increase of speed was decreased by ~4 times (18.8 vs 71 mW/mm^2; Figs. 2*d–h*, 3*g*; contralateral rotations interaction effect$_{\text{light-epoch} \times \text{group}}$: $F_{(2,16)} = 7.849$, $p = 0.0042$; % of contralateral rotations MD, light-ON vs light OFF: ChR2-Sal: 6.0, $p = 0.7009$; ChR2 L-DOPA: 26.20, $p = 0.007$; average speed interaction effect$_{\text{light-epoch} \times \text{group}}$: $F_{(1,8)} = 6.709$, $p = 0.0321$; average speed [cm/s] MD, light-OFF vs light-ON: ChR2-Sal: 0.22, $p = 0.576$ and ChR2 L-DOPA: 0.96, $p = 0.002$; $n = 5$/group, two-way repeated-measures ANOVA). This finding demonstrates that DA neurotransmission directs the

neural circuits toward the motor behavior elicited by activation of M2 neurons.

DA neurons of the SNc receive glutamatergic shaft synapses from cortical regions (Watabe-Uchida et al., 2012). As depolarization of these neurons involves strong recruitment of the major glutamate receptors AMPAR and NMDAR, especially in the dendritic shaft where the evoked postsynaptic potentials are higher than in spine synapses (Jang et al., 2015; Hage et al., 2016), we examined whether antagonism of AMPA and NMDA receptors in SNc neurons would affect the light-induced behavior. Mice carrying AAV5/CaMKII-ChR2-eYFP in the M2 were unilaterally implanted with injection cannulae above the SNc along with an optical fiber into the dmST (Fig. 3*i*,*j*). In the first optogenetic trial, we photostimulated all mice and confirmed the optical fiber placements through the behavior outcomes. One week later, 10 min before the second optogenetic trial, an internal infusion cannula was placed into the mouse's SNc to inject the glutamate antagonists NBQX and AP5 (ChR2-NBQX/AP5 mice), or saline (ChR2-Sal mice). We found that intra-SNc glutamate receptor antagonism only slightly attenuated the contralateral rotations in response to photostimulation (Fig. 3*k*; contralateral rotations interaction effect$_{\text{light-epoch} \times \text{group}}$: $F_{(4,24)} = 1.254$, $p = 0.315$; % of contralateral rotations MD, light-ON vs light OFF: ChR2-Sal: 38.8, $p < 0.001$; ChR2-NBQX/AP5: 20.0, $p = 0.0318$; $n = 5$/group, two-way repeated-measures ANOVA). In contrast, the light-elicited changes in speed were ablated upon antagonist treatment (Fig. 3*l*; average speed interaction effect$_{\text{light-epoch} \times \text{group}}$: $F_{(2,12)} = 12.46$, $p = 0.001$; average speed [cm/s] MD, light-ON vs light OFF: ChR2-Sal: 2.448, $p < 0.01$; ChR2-NBQX/AP5: 0.0820, $p > 0.942$; $n = 5$/group, two-way repeated-measures ANOVA). We hypothesized that selective photostimulation of M2 neurons directly projecting to the SNc (M2-SNc circuit) would evoke speed increments in mice. Accordingly, we injected AAVs containing Cre-dependent ChR2 or EYFP (DIO-ChR2-EYFP and DIO-EYFP, respectively) in M2 and wheat germ agglutinin-Cre (WGA-Cre) in the SNc (Fig. 3*m*). The WGA-Cre expressed in SNc neurons is trans-synaptically transferred to presynaptic terminals (Xu and Südhof, 2013), including those from M2. Using this strategy, the pyramidal M2 neurons that make synaptic contacts in the SNc are labeled with eYFP (Fig. 3*n*). We found that most eYFP-positive neurons reside in the cortical layer 5. We photostimulated the M2 area and observed that, although rotational behavior was unaltered during the light-ON epoch (Fig. 3*o*), M2-SNc-DIO-ChR2 mice exhibited a 30% elevation in average speed upon photostimulation, opposite to that observed on pharmacological silencing of SNc neurons (Fig. 3*p*; average speed interaction effect$_{\text{light-epoch} \times \text{group}}$: $F_{(2,12)} = 22.47$, $p < 0.001$; average speed [cm/s] MD, light-ON vs light OFF: M2-SNc-DIO-eYFP: 0.008, $p = 0.999$; M2-SNc-DIO-ChR2: 1.289, $p < 0.001$; $n = 6–8$/group, two-way repeated-measures ANOVA). Photostimulation of opsin-free mice (M2-SNc-DIO-EYFP) did not alter their locomotion (Fig. 3*o*,*p*). Together, these results suggest that increased velocity, but not rotational behavior, is mediated via M2 neurons projecting to SNc upon optogenetic activation.

Optogenetic stimulation of striatal M2 projections improves motor dysfunction of unilateral dopamine-depleted mice

Depletion of DA reduces the strength of cortical neurotransmission to basal ganglia, which is thought to play a key role in patterning the motor dysfunction in PD (Guo et al., 2015; Mathai et al., 2015; Chu et al., 2017). Although this evidence is the main rationale behind the therapeutic cortical stimulation, the relevant circuit elements within motor cortex likely to disrupt the abnormal activity, and to mediate the therapeutic effects were not demonstrated. Therefore, we investigated whether activation of the M2-dmST circuit could uncover the neural substrates linking cortical stimulation with motor recovery.

We injected mice unilaterally with PBS (dopamine-intact mice) or 6-OHDA (dopamine-depleted mice) into the dmST to induce partial retrograde loss of dopaminergic neurons. We chose the striatum as the route of the neurotoxin administration because this model induces nigrostriatal damage lasting over weeks (Bagga et al., 2015). Mice were randomly assigned to receive viral infusions of AAV5/CaMKIIa-ChR2-eYFP or AAV5/CaMKIIa-eYFP into the M2 (Fig. 4*a*). Mice groups did not differ significantly from each other during the prelesion phase (7 and 3 d before the brain infusions) (Fig. 4*b–f*). However, at the end of the postlesion phase (on the 28th day following brain injection), all unilateral dopamine-depleted mice exhibited impaired forelimb use (Fig. 4*b*; interaction effect$_{\text{time} \times \text{group}}$: $F_{(3,27)} = 13.36$, $p < 0.001$; contralateral forelimb use at day 28 in dopamine-intact [eYFP or ChR2]: 46.89% vs 20.78% in dopamine-depleted [eYFP or ChR2], $p < 0.001$; $n = 13–18$/group, two-way repeated-measures ANOVA) and circling motor abnormalities (Fig. 4*c*; interaction effect$_{\text{time} \times \text{group}}$: $F_{(3,36)} = 7.305$, $p < 0.001$; % of contralateral turns at day 28 in dopamine-intact [eYFP or ChR2]: 53.33% vs 15.13% in dopamine-depleted [eYFP or ChR2], $p < 0.001$; $n = 13–18$/group, two-way repeated-measures ANOVA). These motor dysfunctions showed no evidence of spontaneous recovery over time. We also observed that unilateral dopamine depletion did not result in significant changes in mobility, speed, and total distance traveled over the analyzed period (Fig. 4*d–f*).

Immunoreactivity for TH in four striatal subregions along the AP axis, and the number of TH-positive cells in SNc were significantly reduced on the ipsilateral side to the lesion compared with the contralateral hemisphere Fig. 4*g–j*; TH fluorescence intensity between ipsilateral versus contralateral striatum (MD): 0.86: −97.29, 95% CI −114.4 to −80.13, $t_{(6)} = 13.88$; 0.50: −115.3, 95% CI −127.5 to −103.0, $t_{(6)} = 23.03$; 0.26: −116.8, 95% CI −128.5 to −105.1, $t_{(6)} = 24.42$; 0.14: −111.6, 95% CI −123.4 to −99.76, $t_{(6)} = 23.10$; 3.1-fold reduction of TH-positive neurons in ipsilateral compared with contralateral SNc ($t_{(6)} = 8.44$; $p < 0.001$ in all cases, $n = 4$, Student's t test). Furthermore, depletion of striatal DA and its metabolites was uniform and pronounced in the dopamine-depleted hemisphere (Fig. 4*k*; ipsilateral vs contralateral dorsal striatum [MD in ng/mg of protein]: DA: −0.7585, 95% CI −1.085 to −0.4316, $t_{(6)} = 5.679$; DOPAC: −0.6745, 95% CI −1.023 to −0.3264, $t_{(6)} = 4.741$; HVA: −0.5115, 95% CI −0.6842 to −0.3389, $t_{(6)} = 7.25$; $p < 0.001$ in all cases, $n = 4$, Student's t test).

We then implanted an optical fiber into the dmST and subjected these mice to tests for motor function under photostimulation. As expected, dopamine-depleted mice with either ChR2 or eYFP exhibited similar levels of motor dysfunction during the first light-OFF epoch (Fig. 4*l*,*m*). Notably, optical stimulation did not change the proportion of wall contacts in dopamine-intact mice with ChR2, but it did improve the use of the contralateral paw from 18.8 ± 2.4% to 38.3 ± 3.0% in the dopamine-depleted mice expressing ChR2 during the light-ON epochs (Fig. 4*l*; depleted ChR2 vs eYFP [MD]: 1.45% during light-OFF, $p = 0.9911$; 20.33% during light-ON, $p < 0.001$; $n = 6–10$/group, two-way repeated-measures ANOVA). Strikingly, photostimulation also raised the percentage of contralateral turns from 16.9 ± 4.0% to 41.9 ± 3.7% in dopamine-depleted mice expressing ChR2 (Fig. 4*m*; ChR2 vs eYFP [MD]: 0.05% during light-OFF, $p = 0.9106$; 31.05% during light-ON, $p < 0.001$; $n = 6–10$/group, two-way repeated-measures ANOVA). Indeed, these mice only differed

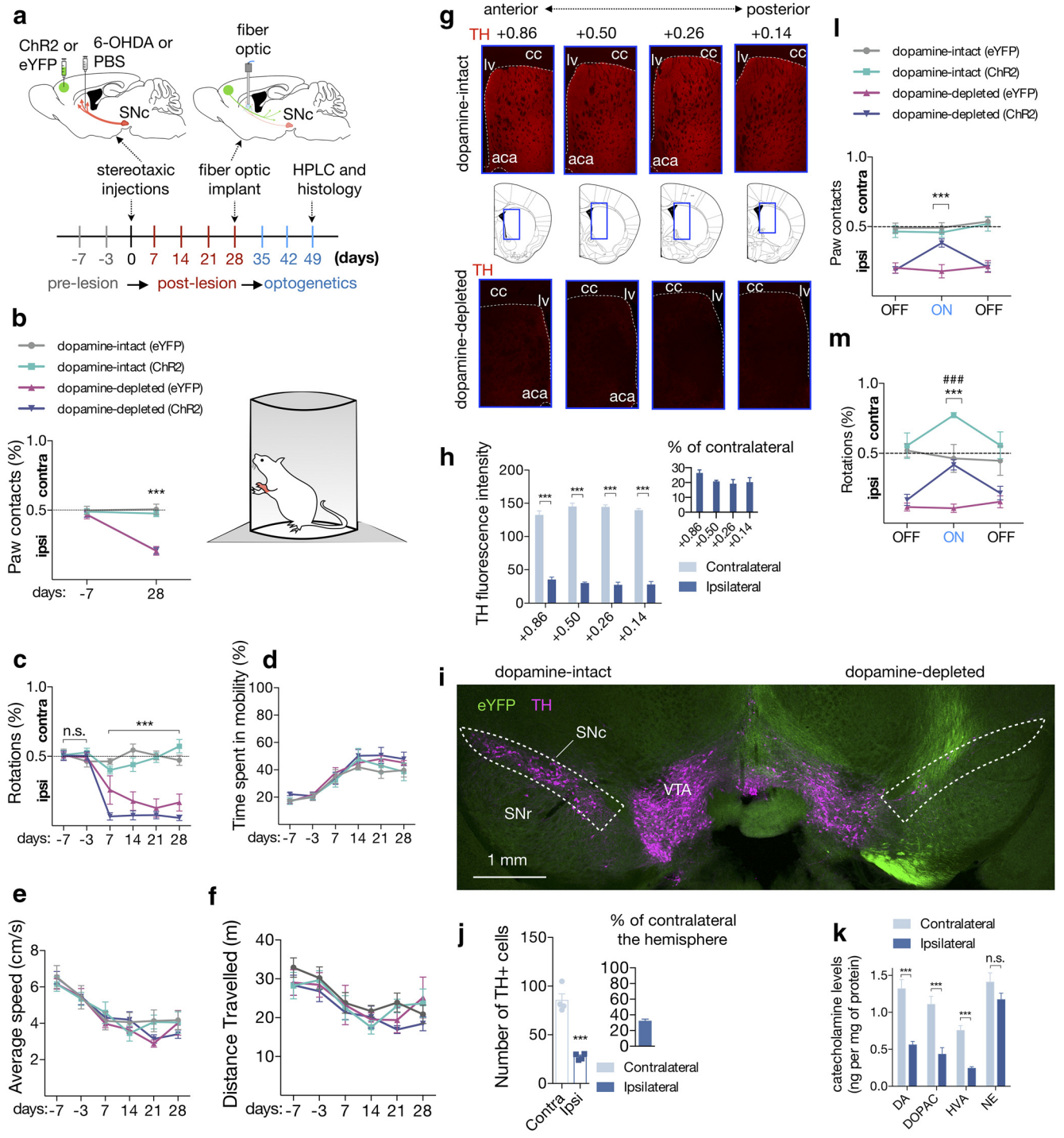

Figure 4. Optogenetic stimulation of M2-dmST projection improves motor dysfunction of unilateral dopamine-depleted mice. ***a***, Top, Experimental scheme to deliver either ChR2 or eYFP into the M2 cortex, and PBS (dopamine-intact) or 6-OHDA (dopamine-depleted) into dorsal striatum. On day 28, when nigrostriatal degeneration is completed, an optical fiber was positioned into the dorsal striatum. Bottom, Timeline of the nigrostriatal lesion, and optogenetics stimulation in the same hemisphere following stereotaxic injections. ***b***, ***c***, All unilateral dopamine-depleted mice exhibited forelimb use asymmetry (cylinder test) and circling motor abnormalities at the end of the postlesion phase: dopamine intact (eYFP): $n = 6$; dopamine intact (ChR2): $n = 7$; dopamine depleted (eYFP): $n = 8$; dopamine depleted (ChR2): $n = 10$. ***d–f***, Unilateral dopamine depletion did not result in significant changes in mobility, speed, and total distance traveled over the analyzed period. ***g***, Representative coronal sections of the dopamine-intact (top) and dopamine-depleted (bottom) mice showing immunoreactivity for TH in four striatal subregions along the AP axis (relative to bregma). lv, Lateral ventricle; cc, corpus callosum; aca, anterior commissure. Red represents TH from immunoreactivity. ***h***, Overall, there was an 80% reduction of TH immunoreactivity in the DA-depleted hemispheres along the AP axis. Inset, Percentage of TH immunoreactivity in ipsilateral relative to the contralateral hemisphere ($n = 4$/group). ***i***, Representative coronal section showing the SNc of the dopamine-intact (left) and the dopamine-depleted hemisphere (right). Green represents eYFP from AAV. Magenta represents TH from immunoreactivity. ***j***, The number of TH-positive cells in the SNc was also significantly reduced in the dopamine-depleted hemisphere. Inset, Percentage of TH-positive cells in ipsilateral relative to the contralateral hemisphere. ***k***, Reduction of striatal levels of DA, DOPAC, and HVA in the dopamine-depleted hemispheres, relative to the intact hemispheres. No significant differences were observed for NE ($n = 4$/group). ***l***, ***m***, Optogenetic stimulation improved the forelimb use asymmetry and circling motor abnormality at the light-ON epoch. ***b***, ***c***, ***l***, ***m***, Dashed line indicates chance performance. In all figures, summary data are indicated as mean ± SEM. $^{***}p < 0.001$. $^{\#\#\#}p < 0.001$.

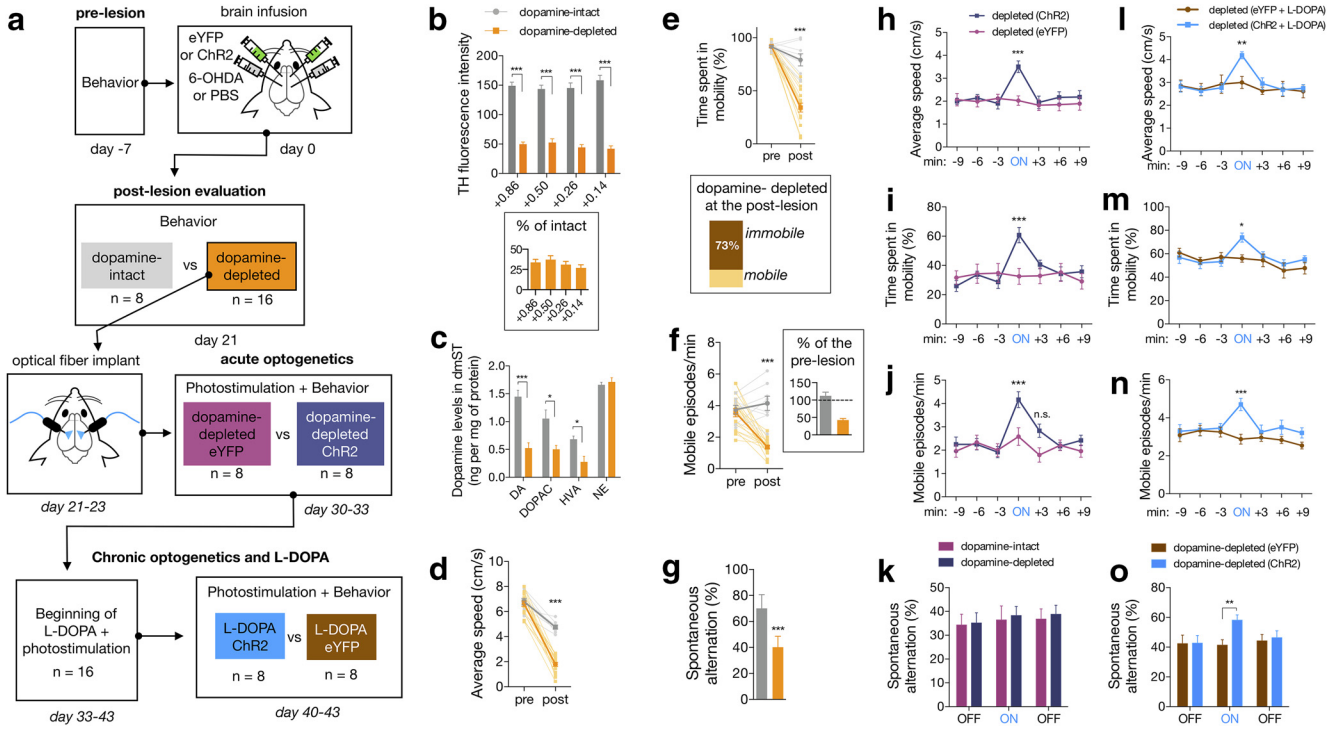

Figure 5. Chronic optogenetic stimulation supplemented with L-DOPA administration ameliorates motor and nonmotor symptoms of bilaterally dopamine-depleted mice. ***a***, Experimental scheme to transfect eYFP or ChR2 in the M2 cortex, and produce the bilateral dopamine-depleted mice ($n = 16$) through injection of 6-OHDA into the dmST. Dopamine-intact mice ($n = 8$) received bilateral injections of PBS in dmST. On day 21, when nigrostriatal degeneration was confirmed (postlesion evaluation), only dopamine-depleted mice received optical fibers positioned into the dmST. These mice underwent an acute photostimulation on days 30–33. Then, L-DOPA and photostimulation were applied in all mice for 7 consecutive days, and another photostimulation trial (chronic) was performed to score the behavior. ***b***, ***c***, In a separate group of animals, we observed that bilateral depleted mice displayed decreases in TH immunoreactivity concentration of dopamine in striatum. ***d–g***, Locomotor behavior and percentage of spontaneous alternation in the Y-maze in DA-intact and DA-depleted mice. ***h–k***, Behavioral effects of acute photostimulation in dopamine-depleted mice expressing either ChR2 or eYFP. Light was delivered for 3 min during the ON epoch. ***l–o***, Behavioral effects of chronic photostimulation supplemented with L-DOPA treatment in dopamine-depleted mice. In all figures, summary data are indicated as mean ± SEM. ***$p < 0.001$. **$p < 0.01$. *$p < 0.05$.

significantly from dopamine-intact mice with eYFP during the light-OFF epochs (Fig. 4*m*; depleted vs intact [MD]: 35.3% during light-OFF, $p < 0.001$; 4.5% during light-ON, $p = 0.9479$). These light-evoked therapeutic benefits were not seen in dopamine-depleted mice carrying eYFP (Fig. 4*l*,*m*). Thus, these findings suggest that stimulation of the M2-dmST circuit is sufficient to improve motor dysfunction in unilateral dopamine-depleted mice.

Chronic optogenetic supplemented with L-DOPA administration ameliorates motor and nonmotor symptoms of bilateral dopamine-depleted mice

Compared with unilateral DA depletion, bilateral lesioned mice reproduce a different spectrum of motor dysfunctions, in addition to cognitive deficits (Rousseaux et al., 2012). We applied the same optogenetic manipulation (acute photostimulation) to test the efficacy of M2 stimulation to revert both motor and nonmotor symptoms of a more pronounced lesioned animal model. Three weeks after the neurotoxin injection (Fig. 5*a*), bilateral dopamine-depleted mice had fewer DA axon fibers in the dmST (Fig. 5*b*; TH intensity in dmST: 33.8 ± 1.6% of control, $p < 0.001$, $n = 4$/group, Student's *t* test), loss of neuronal bodies in the SNc (TH-positive cells in SNc: 28.5 ± 5.6% of control, $p < 0.001$, $n = 4$/group, Student's *t* test), and decreased concentration of striatal DA and its metabolites (Fig. 5*c*; depleted vs intact [MD in ng/mg of protein]: DA: −0.9240, $t_{(6)} = 6.33$, $p < 0.001$; DOPAC: −0.5505, $t_{(6)} = 3.24$, $p = 0.0176$; HVA: −0.4061, $t_{(6)} = 3.616$, $p = 0.011$; NE: 0.053, $t_{(6)} = 0.62$, $p = 0.557$; $n = 4$/group, Student's *t* test). Dopamine-depleted mice also exhibited severe bradykinesia (Fig. 5*d*; average speed [cm/s] in the postlesion phase: intact = 6.79 ± 0.16 vs depleted = 1.78 ± 0.17, $p < 0.001$, $n = 8–18$/group, two-way repeated-measures ANOVA), hypokinesia (Fig. 5*e*,*f*; mobile episodes per minute in the postlesion phase: intact = 4.15 ± 0.45 vs depleted = 1.50 ± 0.20; % of time spent in mobility: intact = 79.95 ± 6.14 vs depleted = 26.46 ± 5.80; in all cases $p < 0.001$, $n = 8–18$/group, two-way repeated-measures ANOVA), and reduced the percentage of spontaneous alternation in Y-maze, which suggests a deficit in spatial working memory (Fig. 5*g*; % of spontaneous alternation in the postlesion phase: intact = 70.03 ± 4.77 vs depleted = 40.21 ± 3.17; $p < 0.001$, $n = 8–18$/group, two-way repeated-measures ANOVA).

All mice from the dopamine-depleted group (eYFP, $n = 8$; ChR2, $n = 8$) were implanted bilaterally with optical fibers into dmST. Ten days later, we submitted the mice to a protocol of acute photostimulation consisting of 9 min of light-OFF, 3 min of light-ON, and another 9 min of light-OFF. The disrupting effects of DA depletion on the locomotor behavior were preserved during the light-OFF epochs in the optogenetic trials (Fig. 5*h–k*). Interestingly, acute photostimulation of ChR2 mice ameliorated all the evaluated locomotor impairments (Fig. 5*h–k*; Movie 2). The most significant improvement observed was a 61.7% increase in average speed (Fig. 5*h*; 2.01 ± 0.17 cm/s in light-OFF vs 3.50 ± 0.25 cm/s in light-ON, $p < 0.001$, $n = 8$/group, two-way repeated-measures ANOVA), indicating an efficient reversal of bradykinesia. Furthermore, during the light-ON epoch, ChR2 mice displayed lower hypokinetic signals as they spent more time being mobile (Fig. 5*i*; 29.4 ± 3.5% in light-OFF vs 60.7 ± 5.26% in light-ON, $p < 0.001$, $n = 8$/group, two-way repeated-measures

Movie 2. Photostimulation of dopamine-depleted mouse expressing ChR2, related to Figure 5*c–g*.

ANOVA), and increased the number of mobile episodes (Fig. 5*j*; 2.1 ± 0.26 in light-OFF vs 4.17 ± 0.34 episodes per minute in light-ON, $p < 0.001$, $n = 8$/group, two-way repeated-measures ANOVA). Conversely, photostimulation of ChR2 mice did not change the deficient percentage of spontaneous alternation in the Y-maze, suggesting that this acute optogenetic manipulation fails to rescue a nonmotor symptom of dopamine depletion (Fig. 5*k*; 35.13 ± 12.10% in light-OFF vs 38.26 ± 10.78% in light-ON for the ChR2 group, $p = 0.988$, $n = 8$/group, two-way repeated-measures ANOVA).

Administration of L-DOPA is the most common treatment for PD patients. This drug increases DA concentrations and compensates for the loss of dopaminergic neurons (Hornykiewicz, 2010). We assessed the intriguing hypothesis whether a chronic optogenetic stimulation of the M2-dmST circuit could potentiate the therapeutic actions of L-DOPA. All mice from the optogenetic acute trial were administered with L-DOPA for 7 consecutive days (daily intraperitoneal injections of 3 mg/kg; Fig. 5*a*). During the course of the pharmacological treatment, we also photostimulated all the mice for 3 min twice a day (between 10:00 A.M. to 12:00 P.M. and 3:00 P.M. to 5:00 P.M.). After the L-DOPA treatment, both ChR2 and eYFP dopamine-depleted exhibited noticeable improvements in locomotor performance (light-OFF of acute vs light-OFF of chronic trials; Fig. 5*h–n*). Although the locomotor behavior of these groups was identical during the light-OFF epoch, L-DOPA-treated ChR2 mice presented a superior locomotor functioning during the photostimulated period (Fig. 5*l–n*; eYFP vs ChR2 during the light-ON: 3.0 ± 0.26 vs 4.19 ± 0.15 cm/s, $p = 0.008$; 55.9 ± 3.1% vs 73.8 ± 3.8% of time spent in mobility, $p = 0.027$; 1.8 ± 0.23 vs 3.45 ± 0.29 mobile episodes per minute, $p < 0.001$; in all cases, $n = 8$/group, two-way repeated-measures ANOVA). Remarkably, locomotor scores in the light-ON after L-DOPA treatment were even greater than previously recorded in the acute light-ON trial (Fig. 5*h–n*). Indeed, most of the locomotor evaluations of L-DOPA-treated ChR2 mice during the light-ON epochs appeared to be very similar to those observed in the intact mice during the postlesion phase (Fig. 5*d–g*). Surprisingly, photostimulation of L-DOPA-treated ChR2 mice also increased the percentage of spontaneous alternations in the Y-maze task, a response that was previously absent with the acute stimulation (Fig. 5*k*,*o*; percentage of alternations of eYFP vs ChR2 during the light-ON: acute optogenetic 36.4 ± 5.87 vs 38.3 ± 3.81, $p = 0.988$; chronic optogenetic with L-DOPA 41.3 ± 3.66 vs 58.1 ± 3.53, $p = 0.037$, two-way repeated-measures ANOVA).

Discussion

We identified a circuit involving long-range glutamatergic projections from the M2 cortex that, when activated, induced locomotion and attenuated the phenotype of dopamine-depleted animal model of PD.

M2 neurons innervate multiple cortical regions but also have dense projections to basal ganglia structures that are involved in the central control of movement (Watabe-Uchida et al., 2012; Gerfen et al., 2013; Hintiryan et al., 2016). It has been challenging to assess the anatomical and functional organization of M2 neurons. These neurons present a remarkable cell type heterogeneity with complex axonal topography that can be vastly biased depending on the output structures (Harris and Shepherd, 2015; Gal et al., 2017). In contrast to the M1 counterpart and its neighboring regions, the behavioral role for M2 neurons remains unclear (Zingg et al., 2014; Barthas and Kwan, 2017). The current understanding suggests that M2 neurons encode sensorimotor associations, implicating the region as a driver of adaptive choice behavior (Murakami et al., 2014; Barthas and Kwan, 2017). Most of the targeted M2 neurons in this study were glutamatergic and projected ipsilaterally to basal ganglia structures implicated in motor control (Fig. 1).

Outside the anatomical ground, quantitative information is still limited toward identifying the top-down control of the behavioral information carried by the M2 projections. This is important as these neurons are multiprojectional, and their functional significance is expected to be diverse. Our manipulations revealed that cell type-specific optogenetic activation of either M2 neuronal bodies or their projection into the dmST evoked locomotion (Fig. 2; Movie 1). Apart from excitatory glutamatergic neurons, the M2 cortex also contains GABAergic neurons projecting to striatal spiny projection neurons (SPNs) (Rock et al., 2016). In contrast to our data, optogenetic activation of somatostatin-positive M2 GABAergic projecting neurons reduced locomotor activity (Melzer et al., 2017). These results are consistent with the notion that the neurochemical diversity of the M2 cortex affects behavior differentially, and possibly may explain why bulk electrical microstimulation of M2 evokes distinct movements of those observed in our study (Donoghue and Wise, 1982; Tennant et al., 2011). Although we attributed the effects of photostimulation to glutamatergic neurons, appropriate caution is warranted when using CaMKII promoters because we cannot exclude the possibility other forebrain neuron types expressed ChR2, as reported previously (Nathanson et al., 2009; Scheyltjens et al., 2015).

Our pharmacological manipulations provided data consistent with the idea that increased locomotion upon stimulation of M2 glutamatergic neurons most likely activates neurotransmission in the basal ganglia. First, optogenetic activation of M2 axons in the dmST was sufficient to evoke locomotor activity (Fig. 2*a–h*).

Second, it is tempting to speculate that photostimulation enhances dopamine release into the dorsal striatum as tissue levels of dopamine and its metabolites DOPAC and HVA were increased in the stimulated hemisphere (Fig. 3*a–c*). Third, dopamine antagonists or replacement therapy (L-DOPA) differently sensitized the light-evoked behavior. Although they did not alter the rotational behavior, DA antagonists decreased the elicited speed changes, whereas L-DOPA appeared to increase the susceptibility to the photostimulation effects (Fig. 3*d–h*). A lower-intensity stimulation protocol (18.8 mW/mm^2) was able to evoke locomotion in L-DOPA-treated mice but did not affect control animals (Fig. 3*h*). Finally, previous studies showed that NMDA and AMPA receptors exert strong control over SNc excitability and motor output via regulation of striatal dopamine release (Jang et al., 2015; Hage et al., 2016). Accordingly, local pharmacological inhibition of glutamatergic receptors in neurons from the SNc blocked the speed increments but not rotational bias in response to M2 activation (Fig. 3*k*,*l*). Interestingly, our dual virus retrograde tracing revealed that M2 neurons provide outputs to SNc neurons that are critical for evoking speed increments but not rotational bias (Fig. 3*m–p*). This strongly suggests that (1) speed control upon M2 activation is at least in part due to direct input from M2 to SNc and (2) expression of distinct locomotor behaviors is dynamically represented in separate subsets of M2 neurons, leaving the open question of which circuit within M2 is preferentially engaged during rotational behavior.

Degeneration of midbrain dopamine neurons in PD patients leads to drastic functional changes within the CBG network, affecting locomotion (including bradykinesia, rigidity, and tremor) and cognitive behavior. Whereas therapeutic targets can be theoretically located at any point of this circuitry, motor symptoms have been partially ameliorated through traditional electrical (Li et al., 2012; de Hemptinne et al., 2015; Lofredi et al., 2018), chemogenetic (Alcacer et al., 2017; Chu et al., 2017), optogenetic (Gradinaru et al., 2009; Kravitz et al., 2010; Kim et al., 2017), and pharmacological (Guo et al., 2015) manipulations targeting primarily basal ganglia structures, such as striatum, STN, and pallidum. Although much progress has been made using these strategies, recent electrophysiology and functional imaging studies suggest that PD symptoms result from alterations in the cerebral cortex, and successful therapies, indeed, encompasses plastic changes in cortical neurons (Dejean et al., 2009; Gradinaru et al., 2009; Li et al., 2012; de Hemptinne et al., 2015; Guo et al., 2015; Chu et al., 2017; Wang et al., 2018). For example, DBS of STN reduced excessive beta phase locking of motor cortex neurons and improved cortical function of PD patients (de Hemptinne et al., 2015). Moreover, the therapeutic effects of spinal cord stimulation on freezing of gait were associated with circuits involving the supplementary motor area (de Lima-Pardini et al., 2018). Therefore, accumulating evidence has proposed that the cortex might be an important target for yielding motor benefit for PD patients, although it remains elusive the salient circuitry substrates relevant for therapy. This study extends this notion by providing the first evidence that activation of M2 neurons is sufficient to attenuate motor dysfunctions of both unilateral and bilateral dopamine-depleted mice. Photostimulation of M2 projections in unilateral depleted mice restored imbalances of rotational behavior in the open field and improved the forelimb use in the cylinder test (Fig. 4). Unlike rotational behavior, this optogenetic manipulation did not change the forelimb use in the control group, suggesting that M2 stimulation elicited antiparkinsonian effects that are dissociable from the induction of voluntary movements. Our acute optogenetic manipulation also improved prominent pathological motor features of bilateral DA-depleted mice, including reductions in voluntary behavior (hypokinesia) and profound slowness of movement (bradykinesia) (Fig. 5*d–h*; Movie 1). However, the acute photostimulation protocol did not recover the working memory impairment detected in the Y-maze (Fig. 5*g*).

We hypothesized that M2 stimulation could supply compensatory signals that counterbalance the CBG dysfunction. Dopamine depletion in humans and experimental models decreases the CBG functional connectivity and the activity of direct pathway spiny projecting neurons (dSPNs) in the striatum, leading to motor impairments (Mathai et al., 2015; Chu et al., 2017; Wang et al., 2018). For example, stimulation of M2 projection can produce dual synaptic activation of dSPNs through M2-dSPN (via glutamatergic excitatory inputs) or M2-SNc-dSPN (via dopaminergic inputs). Photostimulation could, in these circumstances, recover the inhibitory tone of dSPNs on the SNr, ultimately resulting in locomotor activation. Notably, motor neurocircuits are spread and highly redundant. M2 neurons also connected with other basal ganglia structures that can provide parallel sources of functional output from M2 stimulation (Fig. 1). For example, despite the low anatomical connectivity between these regions in our manipulation (2.15%), M2 may activate the STN to control movements. Moreover, it remains yet to be determined whether the M2-STN complementary role reveals why pharmacological blockade of glutamatergic transmission in SNc did not completely cease the elicited behavior. Indeed, identifying the contribution of distinct M2-basal ganglia inputs remains an essential goal for understanding how cortical circuitry selectively engage the motor behavior.

An intriguing finding is that combining L-DOPA treatment with repeated M2 stimulation produced an unanticipated increased performance in Y-maze, measured as the percentage of spontaneous alternation (Fig. 5*o*). In contrast, these procognitive effects were absent in control mice expressing eYFP under L-DOPA treatment or during the acute photostimulation phase. To our knowledge, this provides the first direct demonstration of a cognitive amelioration through optogenetic stimulation of glutamatergic M2 projection into dmST in parkinsonian conditions. Possibly, pairing chronic cortical stimulation with dopamine replacement therapy induces neuroplasticity events that ultimately reinforce working memory (Shen et al., 2015; Grogan et al., 2017). Additionally, these findings led to the hypothesis that M2-basal ganglia circuitry also connect functionally motor and cognitive signals, rather than controlling the execution of movements per se. Our findings therefore pinpoint the possibility that the M2-basal ganglia circuitry can be a relevant anatomical substrate to therapeutic strategies for nonmotor symptoms of PD.

In conclusion, our findings demonstrated that M2 neurons projecting to basal ganglia encode the neural mechanisms of locomotion and establish an optogenetic intervention with the potential to relieve both motor and cognitive symptoms generated by dopamine depletion in the animal model of PD. The present study therefore suggests that activation of the monosynaptic M2 input to basal ganglia can provide new grounds for exploration regarding the therapeutic potential of cortical circuitry in the control of clinical symptoms in PD.

References

Alcacer C, Andreoli L, Sebastianutto I, Jakobsson J, Fieblinger T, Cenci MA (2017) Chemogenetic stimulation of striatal projection neurons modulates responses to Parkinson's disease therapy. J Clin Invest 127:720–734.

Bagga V, Dunnett SB, Fricker RA (2015) The 6-OHDA mouse model of

Parkinson's disease: terminal striatal lesions provide a superior measure of neuronal loss and replacement than median forebrain bundle lesions. Behav Brain Res 288:107–117.

Barthas F, Kwan AC (2017) Secondary motor cortex: where 'sensory' meets 'motor' in the rodent frontal cortex. Trends Neurosci 40:181–193.

Beuter A, Lefaucheur JP, Modolo J (2014) Closed-loop cortical neuromodulation in Parkinson's disease: an alternative to deep brain stimulation? Clin Neurophysiol 125:874–885.

Borchert RJ, Rittman T, Passamonti L, Ye Z, Sami S, Jones SP, Nombela C, Vázquez Rodriguez P, Vatansever D, Rae CL, Hughes LE, Robbins TW, Rowe JB (2016) Atomoxetine enhances connectivity of prefrontal networks in Parkinson's disease. Neuropsychopharmacology 41:2171–2177.

Carbon M, Reetz K, Ghilardi MF, Dhawan V, Eidelberg D (2010) Early Parkinson's disease: longitudinal changes in brain activity during sequence learning. Neurobiol Dis 37:455–460.

Chou YH, Hickey PT, Sundman M, Song AW, Chen NK (2015) Effects of repetitive transcranial magnetic stimulation on motor symptoms in Parkinson disease: a systematic review and meta-analysis. JAMA Neurol 72:432–440.

Chu HY, McIver EL, Kovaleski RF, Atherton JF, Bevan MD (2017) Loss of hyperdirect pathway cortico-subthalamic inputs following degeneration of midbrain dopamine neurons. Neuron 95:1306–1318.e5.

Day M, Wang Z, Ding J, An X, Ingham CA, Shering AF, Wokosin D, Ilijic E, Sun Z, Sampson AR, Mugnaini E, Deutch AY, Sesack SR, Arbuthnott GW, Surmeier DJ (2006) Selective elimination of glutamatergic synapses on striatopallidal neurons in Parkinson disease models. Nat Neurosci 9:251–259.

de Hemptinne C, Swann NC, Ostrem JL, Ryapolova-Webb ES, San Luciano M, Galifianakis NB, Starr PA (2015) Therapeutic deep brain stimulation reduces cortical phase-amplitude coupling in Parkinson's disease. Nat Neurosci 18:779–786.

Dejean C, Hyland B, Arbuthnott G (2009) Cortical effects of subthalamic stimulation correlate with behavioral recovery from dopamine antagonist induced akinesia. Cereb Cortex 19:1055–1063.

de Lima-Pardini AC, Coelho DB, Souza CP, Souza CO, Ghilardi MG, Garcia T, Voos M, Milosevic M, Hamani C, Teixeira LA, Fonoff ET (2018) Effects of spinal cord stimulation on postural control in Parkinson's disease patients with freezing of gait. eLife 7:e37727.

Donoghue JP, Wise SP (1982) The motor cortex of the rat: cytoarchitecture and microstimulation mapping. J Comp Neurol 212:76–88.

Drouot X, Oshino S, Jarraya B, Besret L, Kishima H, Remy P, Dauguet J, Lefaucheur JP, Dollé F, Conde F, Bottlaender M, Peschanski M, Kéravel Y, Hantraye P, Palfi S (2004) Functional recovery in a primate model of Parkinson's disease following motor cortex stimulation. Neuron 44:769–778.

Franklin K, Paxinos G (2008) The coronal plates and diagrams. In: The mouse brain in stereotaxic coordinates. Amsterdam: Elsevier Academic.

Gal E, London M, Globerson A, Ramaswamy S, Reimann MW, Muller E, Markram H, Segev I (2017) Rich cell-type-specific network topology in neocortical microcircuitry. Nat Neurosci 20:1004–1013.

Gerfen CR, Paletzki R, Heintz N (2013) GENSAT BAC cre-recombinase driver lines to study the functional organization of cerebral cortical and basal ganglia circuits. Neuron 80:1368–1383.

Gradinaru V, Mogri M, Thompson KR, Henderson JM, Deisseroth K (2009) Optical deconstruction of parkinsonian neural circuitry. Science 324:354–359.

Grogan JP, Tsivos D, Smith L, Knight BE, Bogacz R, Whone A, Coulthard EJ (2017) Effects of dopamine on reinforcement learning and consolidation in Parkinson's disease. eLife 6:e26801.

Guo L, Xiong H, Kim JI, Wu YW, Lalchandani RR, Cui Y, Shu Y, Xu T, Ding JB (2015) Dynamic rewiring of neural circuits in the motor cortex in mouse models of Parkinson's disease. Nat Neurosci 18:1299–1309.

Hage TA, Sun Y, Khaliq ZM (2016) Electrical and Ca(2+) signaling in dendritic spines of substantia nigra dopaminergic neurons. Elife 5:e13905.

Harris KD, Shepherd GM (2015) The neocortical circuit: themes and variations. Nat Neurosci 18:170–181.

Hintiryan H, Foster NN, Bowman I, Bay M, Song MY, Gou L, Yamashita S, Bienkowski MS, Zingg B, Zhu M, Yang XW, Shih JC, Toga AW, Dong HW (2016) The mouse cortico-striatal projectome. Nat Neurosci 19:1100–1114.

Hornykiewicz O (2010) A brief history of levodopa. J Neurol 257:249–252.

Jang M, Um KB, Jang J, Kim HJ, Cho H, Chung S, Park MK (2015) Coexistence of glutamatergic spine synapses and shaft synapses in substantia nigra dopamine neurons. Sci Rep 5:14773.

Kim IH, Rossi MA, Aryal DK, Racz B, Kim N, Uezu A, Wang F, Wetsel WC, Weinberg RJ, Yin H, Soderling SH (2015) Spine pruning drives antipsychotic-sensitive locomotion via circuit control of striatal dopamine. Nat Neurosci 18:883–891.

Kim J, Kim Y, Nakajima R, Shin A, Jeong M, Park AH, Jeong Y, Jo S, Yang S, Park H, Cho SH, Cho KH, Shim I, Chung JH, Paik SB, Augustine GJ, Kim D (2017) Inhibitory basal ganglia inputs induce excitatory motor signals in the thalamus. Neuron 95:1181–1196.e8.

Kravitz AV, Freeze BS, Parker PR, Kay K, Thwin MT, Deisseroth K, Kreitzer AC (2010) Regulation of parkinsonian motor behaviours by optogenetic control of basal ganglia circuitry. Nature 466:622–626.

Lerner TN, Shilyansky C, Davidson TJ, Evans KE, Beier KT, Zalocusky KA, Crow AK, Malenka RC, Luo L, Tomer R, Deisseroth K (2015) Intact-brain analyses reveal distinct information carried by SNc dopamine subcircuits. Cell 162:635–647.

Li Q, Ke Y, Chan DC, Qian ZM, Yung KK, Ko H, Arbuthnott GW, Yung WH (2012) Therapeutic deep brain stimulation in parkinsonian rats directly influences motor cortex. Neuron 76:1030–1041.

Li Q, Qian ZM, Arbuthnott GW, Ke Y, Yung WH (2014) Cortical effects of deep brain stimulation: implications for pathogenesis and treatment of Parkinson disease. JAMA Neurol 71:100–103.

Lofredi R, Neumann WJ, Bock A, Horn A, Huebl J, Siegert S, Schneider GH, Krauss JK, Kühn AA (2018) Dopamine-dependent scaling of subthalamic gamma bursts with movement velocity in patients with Parkinson's disease. eLife 7:e31895.

Mathai A, Ma Y, Paré JF, Villalba RM, Wichmann T, Smith Y (2015) Reduced cortical innervation of the subthalamic nucleus in MPTP-treated parkinsonian monkeys. Brain 138:946–962.

Melzer S, Gil M, Koser DE, Michael M, Huang KW, Monyer H (2017) Distinct corticostriatal GABAergic neurons modulate striatal output neurons and motor activity. Cell Rep 19:1045–1055.

Mentis MJ, Dhawan V, Feigin A, Delalot D, Zgaljardic D, Edwards C, Eidelberg D (2003) Early stage Parkinson's disease patients and normal volunteers: comparative mechanisms of sequence learning. Hum Brain Mapp 20:246–258.

Murakami M, Vicente MI, Costa GM, Mainen ZF (2014) Neural antecedents of self-initiated actions in secondary motor cortex. Nat Neurosci 17:1574–1582.

Nathanson JL, Yanagawa Y, Obata K, Callaway EM (2009) Preferential labeling of inhibitory and excitatory cortical neurons by endogenous tropism of adeno-associated virus and lentivirus vectors. Neuroscience 161:441–450.

Oh SW, Harris JA, Ng L, Winslow B, Cain N, Mihalas S, Wang Q, Lau C, Kuan L, Henry AM, Mortrud MT, Ouellette B, Nguyen TN, Sorensen SA, Slaughterbeck CR, Wakeman W, Li Y, Feng D, Ho A, Nicholas E, et al. (2014) A mesoscale connectome of the mouse brain. Nature 508:207–214.

Parker PR, Lalive AL, Kreitzer AC (2016) Pathway-specific remodeling of thalamostriatal synapses in parkinsonian mice. Neuron 89:734–740.

Pasquereau B, Turner RS (2011) Primary motor cortex of the parkinsonian monkey: differential effects on the spontaneous activity of pyramidal tract-type neurons. Cereb Cortex 21:1362–1378.

Piano C, Fasano A, Daniele A, Di Giuda D, Ciavarro M, Tufo T, Zinno M, Bentivoglio AR, Cioni B (2018) Extradural motor cortex stimulation improves gait, speech, and language in a patient with pure akinesia. Brain Stimul 11:1192–1194.

Rock C, Zurita H, Wilson C, Apicella AJ (2016) An inhibitory corticostriatal pathway. Elife 5:e15890.

Rousseaux MW, Marcogliese PC, Qu D, Hewitt SJ, Seang S, Kim RH, Slack RS, Schlossmacher MG, Lagace DC, Mak TW, Park DS (2012) Progressive dopaminergic cell loss with unilateral-to-bilateral progression in a genetic model of Parkinson disease. Proc Natl Acad Sci U S A 109:15918–15923.

Sanders TH, Jaeger D (2016) Optogenetic stimulation of cortico-subthalamic projections is sufficient to ameliorate bradykinesia in 6-OHDA lesioned mice. Neurobiol Dis 95:225–237.

Scheyltjens I, Laramée ME, Van den Haute C, Gijsbers R, Debyser Z, Baekelandt V, Vreysen S, Arckens L (2015) Evaluation of the expression pattern of rAAV2/1, 2/5, 2/7, 2/8, and 2/9 serotypes with different promoters in the mouse visual cortex. J Comp Neurol 523:2019–2042.

Shen W, Plotkin JL, Francardo V, Ko WK, Xie Z, Li Q, Fieblinger T, Wess J, Neubig RR, Lindsley CW, Conn PJ, Greengard P, Bezard E, Cenci MA, Surmeier DJ (2015) M4 muscarinic receptor signaling ameliorates striatal plasticity deficits in models of L-DOPA-induced dyskinesia. Neuron 88:762–773.

Shepherd GM (2013) Corticostriatal connectivity and its role in disease. Nat Rev Neurosci 14:278–291.

Tennant KA, Adkins DL, Donlan NA, Asay AL, Thomas N, Kleim JA, Jones TA (2011) The organization of the forelimb representation of the C57BL/6 mouse motor cortex as defined by intracortical microstimulation and cytoarchitecture. Cereb Cortex 21:865–876.

Udupa K, Bahl N, Ni Z, Gunraj C, Mazzella F, Moro E, Hodaie M, Lozano AM, Lang AE, Chen R (2016) Cortical plasticity induction by pairing subthalamic nucleus deep-brain stimulation and primary motor cortical transcranial magnetic stimulation in Parkinson's disease. J Neurosci 36:396–404.

Wang YY, Wang Y, Jiang HF, Liu JH, Jia J, Wang K, Zhao F, Luo MH, Luo MM, Wang XM (2018) Impaired glutamatergic projection from the motor cortex to the subthalamic nucleus in 6-hydroxydopamine-lesioned hemi-parkinsonian rats. Exp Neurol 300:135–148.

Watabe-Uchida M, Zhu L, Ogawa SK, Vamanrao A, Uchida N (2012) Whole-brain mapping of direct inputs to midbrain dopamine neurons. Neuron 74:858–873.

Weiss D, Klotz R, Govindan RB, Scholten M, Naros G, Ramos-Murguialday A, Bunjes F, Meisner C, Plewnia C, Krüger R, Gharabaghi A (2015) Subthalamic stimulation modulates cortical motor network activity and synchronization in Parkinson's disease. Brain 138:679–693.

Wu T, Hallett M (2005) A functional MRI study of automatic movements in patients with Parkinson's disease. Brain 128:2250–2259.

Xu W, Südhof TC (2013) A neural circuit for memory specificity and generalization. Science 339:1290–1295.

Yang L, Beal MF (2011) Determination of neurotransmitter levels in models of Parkinson's disease by HPLC-ECD. Methods Mol Biol 793:401–415.

Zeighami Y, Ulla M, Iturria-Medina Y, Dadar M, Zhang Y, Larcher KM, Fonov V, Evans AC, Collins DL, Dagher A (2015) Network structure of brain atrophy in de novo Parkinson's disease. eLife 4:e08440.

Zingg B, Hintiryan H, Gou L, Song MY, Bay M, Bienkowski MS, Foster NN, Yamashita S, Bowman I, Toga AW, Dong HW (2014) Neural networks of the mouse neocortex. Cell 156:1096–1111.